# Architecture and unit design of a capital cost optimized, household electrodialysis desalination device with continuous flow

by

Hannah M. Varner

Submitted to the Department of Mechanical Engineering
in partial fulfillment of the requirements for the degree of

Master of Science in Mechanical Engineering

at the

MASSACHUSETTS INSTITUTE OF TECHNOLOGY

September 2020



Author .....
Department of Mechanical Engineering
August 27, 2020

Certified by .....
Amos G. Winter, V
Associate Professor of Mechanical Engineering
Thesis Supervisor

Accepted by .....
Nicolas Hadjiconstantinou
Professor, Graduate Officer

# Architecture and unit design of a capital cost optimized, household electrodialysis desalination device with continuous flow

by

Hannah M. Varner

Submitted to the Department of Mechanical Engineering
on August 27, 2020, in partial fulfillment of the
requirements for the degree of
Master of Science in Mechanical Engineering

## Abstract

Improved solutions for water desalination are necessary in the urban Indian setting. Currently, a majority of point-of-use (POU) purifiers use reverse osmosis (RO) to desalinate household water. However, RO purifiers waste up to 70% of the feed water when used in the domestic context. Electrodialysis (ED) is a water-efficient alternative means of desalination that preserves >80% of the feed as product water. Though it has been proposed previously and is used in industrial processes, ED has not been successfully implemented for domestic POU desalination in India or globally. This work aims to understand how ED systems can be modified to the POU scale and, critically, how they can be made cost competitive to RO systems. We do this by proposing and then validating a new, direct-flow continuous ED architecture with differential flow rates (and pressures) between the diluate and concentrate channels. This architecture is made possible by a small ED stack, which can withstand a flow channel pressure imbalance. Using numerical system models, a system design was optimized for minimum capital cost, informed by design requirements for a characteristic Indian usage context. A prototype of this system was capable of a 37±6% reduction in feed water salinity from (1500±20 to 940±140 mg/L) at ≥90% water recovery and incorporated electrodialysis reversal and acid dosing as mechanisms to enhance reliability and prevent mineral scaling. If realized as a commercial POU product, ED has the potential within the Indian market to conserve >200 million liters of water per day if adopted in place of low-recovery RO purifiers among even a small fraction of high-income Indian households.

Thesis Supervisor: Amos G. Winter, V
Title: Associate Professor of Mechanical Engineering

# Acknowledgments

To everyone who helped me through this process, thank you.

To my advisor, Dr. Amos Winter, for showing me what research is and for welcoming me into the development engineering community. To all of my friends and peers in the Global Engineering and Research (GEAR) Lab, you have been my first line of defense from all the trials and tribulations of grad school, and the best intellectual and emotional support I could have asked for. Especially to the 'Desal Team' and Sahil Shah as my mentor in all things electrodialysis. I couldn't have tackled these research questions without your eternal patience and guidance. To Elliott Donlon and Dr. Julia Sokol for being the squad that got us through our final push together. To Rashed Al-Rashed for humoring every single odd-hours rambling question I could come up with and for the revisions that made me happy to read. To Dr. Kameron Conforti for so patiently teaching me electro-chemistry. To my electronics and controls **saviors** Jeff Costello, Elizabeth Brownell and Shane Pratt: I would be doing all my calculations with an abacus if not for you. And to every other member of the GEAR lab too for giving me wisdom and guidance when I was stuck or struggling, joy and laughter when I needed it most, and for stretching me to see the diversity of what grad school can be, thank you.

To the team at Eureka Forbes Ltd: Mr. Suresh Redhu, Dr. SK Sankar, Dr. Sathish Kumar and Dr. Swathy J.R., thank you for believing in this research and for so graciously welcoming me to your offices. You made me feel at home in Bangalore even with August heat and a broken foot.

To my parents and to Max, for being my cheerleaders and sounding board, and for taking care of me when I went down the rabbit hole of grad school.

THIS PAGE INTENTIONALLY LEFT BLANK

# Contents

# List of Figures

# List of Tables

THIS PAGE INTENTIONALLY LEFT BLANK

# Chapter 1

# Introduction

## 1.1 Motivation

The objective of this work is to understand how electrodialysis (ED) systems can be designed and optimized for point-of-use brackish water applications. Water scarcity is a global concern and is particularly relevant in India, where the government rates only 63% of their communities as having access to safe groundwater reserves [1]. To meet water demand across the country, water sources of lower quality, including brackish groundwater (with >3,000 mg/L total dissolved salts (TDS)) or biologically contaminated surface waters, are frequently tapped to supplement or replace inconsistent municipal supplies. Desalination of brackish groundwater to a potable salinity (<500 mg/L TDS) is necessary to meet World Health Organization guidelines for safe drinking water [2].

The variable quality of water from different sources, and the need for desalination, results in the broad installation of point-of-use (POU) water purifiers, particularly in urban Indian households. Over 35% of new POU purifiers sold in India rely on reverse osmosis (RO) [3]. When used at a domestic scale, RO purifiers do not incorporate energy recovery or high water recovery technology that is common for industrial implementations. As a result, the water recovered from a supplied feed volume averages around 26% [4] and energy usage is

significantly higher than large scale municipal desalination [5].

In 2018, Frost and Sullivan estimated only 4% of consumers in India owned a POU water purifier; however, new POU purifier sales were predicted to grow at a rate of 15% per year through 2023 [3]. This would result in over 8 million purifiers sold annually, 2.7 million of which will be using RO. If just 10% of the top two socio-economic groups in India adopted POU RO purification, over 234 million liters of water would be wasted *every day* due to current systems' low recovery [6]. These inefficiencies, combined with the water shortage across the country and the growing purifier market, have led to proposed legislation from the National Green Tribunal of India that would completely ban the use of RO POU devices in low salinity applications and impose higher recovery requirements on all POU purification [7].

Electrodialysis is an alternative method of desalination that can provide higher water recovery and energetic efficiency than RO for brackish water desalination at the POU scale [8]. ED is an established technology in industrial-scale applications with flow rates exceeding 1,000 $m^3$ per day and diverse applications from food and wastewater processing to manufacturing as well as drinking water [9, 10, 11, 12]. However, ED has not been successfully deployed at domestic scales, where daily water requirements are under 0.1 $m^3$ per day. Previous research has attempted to scale ED systems to POU size by either using batch processing or by staging ED with RO [13, 14, 15], but neither architecture has been commercially adopted. Additional architecture variations may provide ED systems that align with market-driven requirements.

Applying ED in a domestic setting is also challenging because capital cost becomes equally important to technical function. Domestic POU water purifiers are consumer items; therefore, the end user is highly sensitive to the purchase price. In their assessment of the Indian market, Frost and Sullivan rate customer sensitivity to price at 9 out of 10 for POU purifiers [3]. Capital cost reduction of the ED unit is critical to ensuring that customers will purchase the product, and that the manufacturer of an ED POU system has the required profit margin

to make the product viable.

The key questions addressed in this study are:

1. What are the market-driven design requirements that could enable the success of a POU ED water purifier with respect to cost competitiveness, reliability, and manufacturer interest?

2. How can a parametric understanding of ED lead to previously unexplored POU system architectures?

3. Can a new design be validated to meet the market-driven design requirements?

## 1.2 Design requirements

Through on-the-ground observation and a collaboration with Eureka Forbes Ltd, the market leader in POU RO systems in India, we divided major design requirements of POU ED systems into 1) customer-facing production metrics, 2) environmental factors (water quality), 3) system operation limits, and 4) manufacturer-facing installation and fabrication factors. Table 1.1 summarizes these efforts and quantifies the key requirements that an ED desalination unit would need to meet in order to successfully integrate into the Indian domestic purifier landscape.

The listed recovery ratio of 90% was selected to respond to the need to conserve resources, described above, and to capture the new value proposition to customers of an ED-based purifier that requires less input water. An evaluation of the willingness to pay of likely consumers has shown that high water recovery is the most significant factor influencing a consumer's perceived utility of the purifier [6]. The impact was measured at 68% compared to 12% for cost, 11% for power rating and 10% for annual maintenance.

Table 1.1: Functional design requirements and constraints for a POU ED system for the Indian market. Unless otherwise noted, these requirements were articulated by Eureka Forbes Ltd, the market leader in Indian POU RO systems [16].

| Variable | Requirement | Justification |
|---|---|---|
| | *Product water* | |
| Flow rate | 12-15 L/h | Typical of commercial POU RO systems in India |
| TDS reduction | ≥90% (min 50 mg/L) | Comparable with bottled water in India [17] |
| Recovery ratio | ≥90% | |
| | *Feed water specifications* | |
| TDS | 500-2000 mg/L | See Table 1.2 |
| Operational TDS variability | ±500 mg/L | Day to day and seasonal variability |
| Alkalinity | pH ≤7.4-7.8 | Typical as observed by Eureka Forbes |
| | *System operation* | |
| Operational cost | Unconstrained | Unspecified as a constraint. ≤Wattage of other household appliances preferred [6] |
| ED-specific component volume | ≤6L | Double the volume of RO components targeted for replacement by ED in existing POU purifiers |
| Pressure drop | ≤1 bar | Targeting lower cost and lower power pumps than POU RO systems |
| Voltage | <24 V | Typical power to POU RO systems |
| | *Manufacturing and installation* | |
| System component count | Minimize | Assembly process is manual and non technical |
| System component type | Off-the-shelf preferred | Leverage existing high-volume components with economies of scale and existing supply chains |
| Module form | Housing form factor maintained | Wall-mounted housing exterior is the same injection mold used in current RO systems. Interior changes only to accommodate the new desalination system |
| Module to housing integration | Clear electrical and hydraulic connections | More complicated assembly needs than current POU RO devices would require retraining of current assembly workers |
| Robust design | Withstand transit | Delivery chain is not temperature regulated or vibration isolated. Components and connections (electric and hydraulic) must survive transit |
| Customer installation | Straightforward | Occurs in residential homes: should not require specialized hardware, power, or training to the installation technicians |
| Functional similarity | Single pass water delivery | Same as POU RO units now |
| Operational reliability | High reliability for TDS and production volume over a long duration | Company reputation depends on reliability of the device. Customers expect POU RO to last up to 15 years[6]. |
| Hazardous chemicals | Forbidden | Consumer product in homes cannot have hazardous chemical (including HCl) |
| Service interval | ≥6 months | Current schedule used on POU RO units |

Water quality standards and customer expectations drive target TDS reduction. An understanding of the Indian market, as collected by Eureka Forbes and shown in Table 1.2, informed the likely composition of the feed water. Though the specific feed water parameters presented here were reported by Eureka Forbes, the ranges are comparable to those seen globally for brackish water [18].

Table 1.2: Water supply salinity of potential customers of Eureka Forbes. A majority of households tested to have under 400 mg/L total dissolved salts.

| TDS Estimated mg/L | Households % |
|---|---|
| <400 | 76% |
| 400-1000 | 20% |
| >1000 | 4% |

While customers indicate a willingness to pay for a higher recovery POU purifier, a low capital cost technology to achieve this is required for manufacturers to view this as a profitable choice. Therefore, capital cost was used as the optimization objective in determining the system design and is excluded from the design requirements listed in Table 1.1. By contrast, the unconstrained specific energy consumption (and therefore operational cost) is considered a design parameter but is not significant enough to final product viability to place a threshold.

Eureka Forbes indicated that after capital cost, the second most important aspect of a potential ED design would be how well the unit integrated into current production practices, in service operation, and the maintenance framework of the company. The latter portion of Table 1.1 lists the manufacturing and installations brought about by Eureka Forbes' market insights. Four significant themes emerged that provided insight into the difficulty of implementing ED in POU applications including: 1) manufacturing line and maintenance technician unfamiliarity with the water flow diagram and required inputs/outputs of an ED system, 2) the brand recognition and consumer expectation for the exterior POU unit size/integration into wall mounted purifiers, 3) the reliability of an ED system to provide

consistent water quality without fouling or clogging, and 4) the ability to survive the rough shipment and climate handling common for RO systems in use now. A design that is responsive to these additional four considerations would have the highest likelihood for successful uptake in the market.

The goal of incorporating market-derived constraints at the outset of the technical design considerations was to avoid unexpected barriers to implementation and uptake at the initial analysis stages for the design. For example, when considering reliability, fouling and clogging are common concerns in RO systems that have analogous failure mechanisms in ED. Mineral ions are abundant in groundwater (e.g. calcium and magnesium carbonates) and these ions can cause harmful mineral scale deposits within ED systems [19]. Acid dosing is preferred to chemical softening in ED systems, but POU systems are constrained further to use only methods and chemicals that are safe for a domestic setting. Previous research assessing POU ED system feasibility has, in large part, not considered the additional complications of scale mitigation in the system design, cost and size [13, 14, 15, 20]. Requiring reliable system performance in mineral containing water leads to additional costs and complexities that inform which design is best matched for the POU application.

The overall cost of a POU ED system is calculated based on a summation of the capital costs for the main functional components of the system as

$$CC_{\text{total}} = CC_{\text{filtration}} + CC_{\text{scale mitigation}} + CC_{\text{hydraulic,electrical}} + CC_{\text{ED stack}}. \tag{1.1}$$

Having determined realistic constraints and bounds for this equation in the context of POU ED, the remainder of this work seeks to determine the POU ED design that minimizes our primary system objective, $CC_{\text{total}}$.

# Chapter 2

# ED behavior and size-scale insights

In this chapter we outline the key functional components of an ED system, describe the mechanisms of desalination in ED, and use insights from this physics-based description to propose a new architecture for an ED-based desalination system.

## 2.1 ED components

An ED unit is comprised of a *stack* containing the ion separation membranes and a voltage supply that provides the driving potential for desalination (Fig. 2-1). In the presence of an applied field, charged ions will flow towards the anion or cation of the stack system. The ion exchange membranes (IEM) are selectively permeable to either cations (cation exchange membranes, CEM) or anions (anion exchange membrane, AEM). Water flows between the IEMs in a mesh spacer. As ions are pulled by the applied potential, the membranes block ions of the opposite charge. By alternating a CEM and AEM around flow spacers, channels of concentrate (reject) and diluate (product) water are created. One unit of AEM, CEM and two spacers is known as a *cell pair*.

The rate of desalination within a stack is determined by the geometry and configuration of the cell pairs. Changing flow path geometries (length $L$, width $W$, and height $h$) will affect the linear flow velocity of water within the stack. This results in changes to the Reynolds

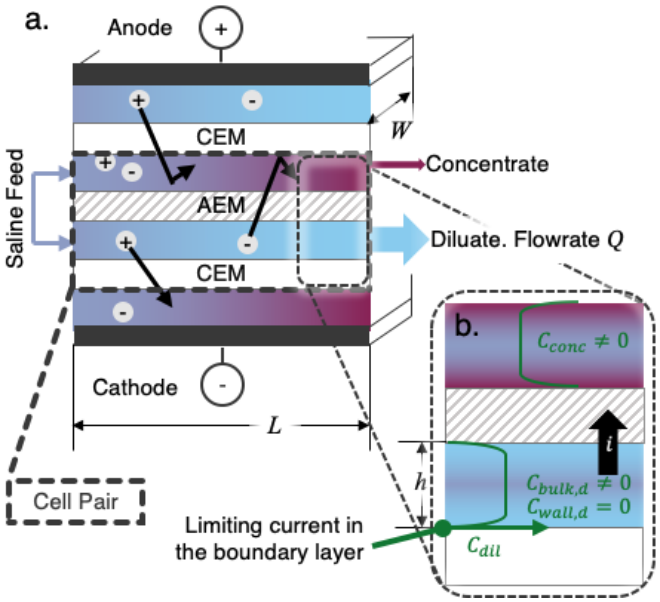


Figure 2-1: Electrical detail of ion flow within stack of ED membranes and spacers. **a.** Ions are subject to an applied current and separated by selectively permeable membranes. A cell pair unit (dashed border) consists of an AEM and CEM. Saline feed at a cell pair flow rate, $Q$, flows the length of the stack, $L$, and leaves the stack as concentrate and diluate. **b.** Diffusion-limited transport at the fluid-membrane interface causes concentration polarization. This phenomenon imposes a limiting current.

number and relative advective, viscous, and diffusive mixing within the channels [21]. The number of cell pairs, $N$, will influence the overall power required for desalination, as each channel and membrane acts as a resistive element in the circuit.

Desalination rate is limited by the diffusion and mixing of ions within the channels. As the applied current density, $i$ [A/m$^2$], is increased, ions are removed from the boundary layers of the diluate stream until they are removed faster than they can be replenished by either diffusion or water mixing, as is shown in Fig. 2-1b. The limiting current density $i_{lim}$, is the current density at which the salt concentration at the IEM surface reaches zero. At $i_{lim}$, salt ions are no longer present to carry the ionic current that the applied voltage mandates. Thus, water is hydrolized into $H^+$ and $OH^-$ in the depleted regions near the membranes in order to provide ions to carry the current. This water splitting causes pH changes of the product water and an increased tendency for mineral scale deposits (primarily $CaCO_3$) to occur in basic regions. As mineral scale precipitates and accumulates in the system, the

IEMs may become ineffective (with reduced flow volume or reduced ion permeability).

## 2.2 Parametric equations for ED behavior

A number of parametric equations have been established to describe and assess ED performance [22, 21]. Here we present a subset of these equations that are useful in considering the success of potential new ED designs. To understand how we can minimize cost, we must first consider the electrical description of an ED stack.

### 2.2.1 Electrical resistance and mass transfer

It is useful to consider the stack as a circuit, where each membrane and channel contributes a resistance and the redox reactions at the electrodes and the IEMs contribute to an additional voltage drop, $E_{el}$ and $Emem$, respectively. When taken together, the total voltage, $E$, is directly proportional to the number of cell pairs, $N$, per

$$E = E_{el} + N(E_{mem} + i(R_d + R_c + R_{mem})), \tag{2.1}$$

where $i$ [A/m$^2$] is the *local* current density in the flow path. The total current flowing between the electrodes $I_{total}$, is the integral of $i$ over the flow path area. The resistance of the diluate and concentrate channels, $R_d$ and $R_c$ [$\Omega$·m$^2$], respectively, is proportional to the channel height $h$ and inversely proportional to the conductance, $\Lambda$ [S· m$^2$/mol], and concentration of the channel in question, $C_d/c$ [mol/m$^3$], at the wall. This is given by

$$R_{d/c} = \frac{h}{\Lambda C^w_{d/c}}. \tag{2.2}$$

The rate of change in the bulk concentration for a given volume of water ($V_d \frac{\mathrm{d}C^b_d}{\mathrm{d}t}$ [mol/m$^3$s]) is related to the area over which the current is applied. Converting $i$ from [A/m$^2$] to [mol

$e^-$] this becomes

$$V_d \frac{dC_d^b}{dt} = \frac{-i}{zF} \phi L W N, \tag{2.3}$$

where the ion valency, $z$, and the Faraday constant, $F$, are known electrical inputs. Note the inclusion of $\phi$, the open-area fraction of the spacer mesh (in the direction of current flow) in specifying the true area over which current can travel in the flow channels.

The maximum current that can be applied to a stack is limited by the diffusion of ions to the membrane surface. This 'limiting current density,' $i_{lim}$, relates the bulk concentration of the diluate, $C_d^b$, to the wall concentration at the membrane, $C_d^w$, using a stack-specific mass transfer coefficient $k$. For this relation we must include the ion transport number through the bulk, $t_{+,-}$, and counterion transport within the membranes, $t^{AEM,CEM}$=1, to obtain

$$i_{lim} = \frac{C_d^b z F k}{t^{AEM,CEM} - t_{+,-}}. \tag{2.4}$$

Recalling that the ratio of convective mass transfer to diffusive mass transfer is the dimensionless Sherwood number, $Sh$, it is observed that in the boundary layer $k$ is given by

$$k = \frac{Sh D_{aq}}{d_h}, \text{ where} \tag{2.5}$$

$$d_h = \frac{h\epsilon}{2 + 8(1-\epsilon)}. \tag{2.6}$$

While the diffusivity, $D_{aq}$, is a material property of water, the hydraulic diameter, $d_h$, depends on the mesh properties of channel height, $h$, and volume porosity of the spacer ,$\epsilon$. $Sh$ further depends on both the mesh and hydrodynamic properties of the system. A number of correlations have been empirically determined to connect $Sh$ to the flow within woven spacers [23, 24, 25]. These correlations relate mass transport, advection and diffusion in woven spacers through the dimensionless quantities of Reynolds number

$$Re = \frac{\rho_{aq} u_{ch} d_h}{\mu} \propto \frac{\text{inertial forces}}{\text{viscous forces}}, \tag{2.7}$$

and Schmidt number (a material property of water at a given temperature)

$$Sc \propto \frac{\text{viscous forces}}{\text{diffusive forces}}, \tag{2.8}$$

to produce a relation of the form

$$Sh = 0.29 Re^{0.5} Sc^{0.33}. \tag{2.9}$$

Equation 2.9 is presented with coefficients determined by Geraldes et al. [25]. In this correlation, the velocity is the linear 'channel' velocity of the flow as it travels around the spacer mesh $u_{ch} = u_v/\epsilon$, and $u_v$ is given by

$$u_v = \frac{Q}{NWh}, \tag{2.10}$$

where $N$, $W$, and $h$ are the previously described cell pair number and flow path geometry, and $Q$ is the volumetric flow rate in the channel.

### 2.2.2 Parametric system characterization

Maintaining a pressure drop <1 bar is another important requirement defined for a POU ED stack. Previous work by Wright et al. [21] has shown the pressure correlation developed by Ponzio et al. [26] for flow through woven spacers provides good correlation in a range of ED stack sizes. This correlation, described in Eq. 2.11, relies on the channel flow velocity in the absence of any spacer ($u_v$, Eq. 2.10), the system production rate, $Q_{prod}$, the geometry and configuration of the channels, and an empirically derived friction factor $f$. From these it can be seen that pressure drop scales as $1/h^3$ given $u_v \propto 1/h$ and $\Delta P \propto u_v^2/h$.

$$\Delta P = \frac{\rho_{aq} f L u_v^2}{4h} \tag{2.11}$$

As with any desalination process, energy is required to separate the salt from the feed water. The specific energy consumption (SEC, $\Gamma$) is the total energy per unit flow product ($Q_p$) in units of kWh/m$^3$. The two principal components of SEC are 1) the pumping power $\Gamma_{pump}$, and 2) the energy required for desalination (applied to the stack) $\Gamma_{desal}$. Using the earlier equations to calculate the total voltage and current applied to the stack ($E_{total}$ and $I_{total}$) we can produce the first term of SEC,

$$\Gamma_{desal} = \frac{E_{total} I_{total}}{Q_{prod}}. \tag{2.12}$$

Obtaining a relation for the pressure allows us to predict $\Gamma_{pump}$ assuming an assumed efficiency ($\eta_{pump}$) of the pump.

$$\Gamma_{pump} = \frac{(Q_{prod} + Q_{reject})\Delta P}{\eta_{pump} Q_{prod}} \tag{2.13}$$

In addition to the energetic implications of pressure, it is also useful to consider how pressure influences the structural integrity of the stack. Of particular concern is damage to the membranes that can arise from deflection due to pressure differences across them. Though the channel spacers ensure that any deflection present is bounded by the mesh thickness, to understand the impact of pressure on the spacers it is useful to approximate a spacer in plane stress as a fixed-fixed beam with a distributed load, $\omega$ [N/m]. Assuming the span is long compared to the channel height ($W \gg h$), and the membrane has a second moment of area, $I$ and Young's modulus, $E$, the deflection is described as

$$\delta_{mem} \propto \frac{W^4 \omega}{EI}. \tag{2.14}$$

For a rectangular cross sections, $I \propto Lt^3$ where $t$ is this thickness of the membrane. Rearranging the terms in Eq. 2.14, we see that $\frac{W^4}{\delta_{mem}} \propto \frac{Et^3}{P}$. Therefore, for a fixed membrane material, thickness, and pressure, small decreases in the span, $W$, lead to large decreases in

the deflection.

## 2.3 ED system architectures

### 2.3.1 Conventional architectures

In practice, the surrounding architecture of an ED stack directly dictates the overall performance and function of a POU purifier. Enabling ED at a POU scale requires additional consideration of this architecture for the water circulation system, as these components add cost and volume that may result in a system's inability to meet the design requirements of Table 1.1.

The first circulation variant to consider is a batch water delivery system (Fig. 2-2a). In this system, diluate and concentrate recirculate through parallel flow loops until the desired salinity is achieved and then transferred to a storage tank (or disposed of) in one 'batch'. A tank and a pump are required for each flow stream in this configuration. By contrast, Fig. 2-2b depicts an architecture that enables continuous water delivery in a feed-and-bleed configuration. In this variant, the product tank is continuously filled when the system is running. Concentrate is recirculated in a small amount ('bled' back to the system) in order to achieve a recovery ratio >50%.

Both architectures depicted include valve networks to allow for reversal of the diluate and concentrate streams (inset of Fig. 2-2). Electrodialysis reversal (EDR) is a common tactic used to prolong the life of the membranes through periodically reversing the electrode polarity (inverting the anode and cathode of Fig. 2-1). This inversion between operational 'positions' switches which channels of the stack collect diluate and concentrate, and allows for mineral deposits that may have begun nucleation in the concentrate stream to be dissolved away in the unconcentrated diluate stream [27, 28]. Specialized valves exist for performing this operation on industrial-scale systems; however, similar flow diverters are not common at the POU scale flow rates, necessitating the solenoid valve (SV) network shown as the

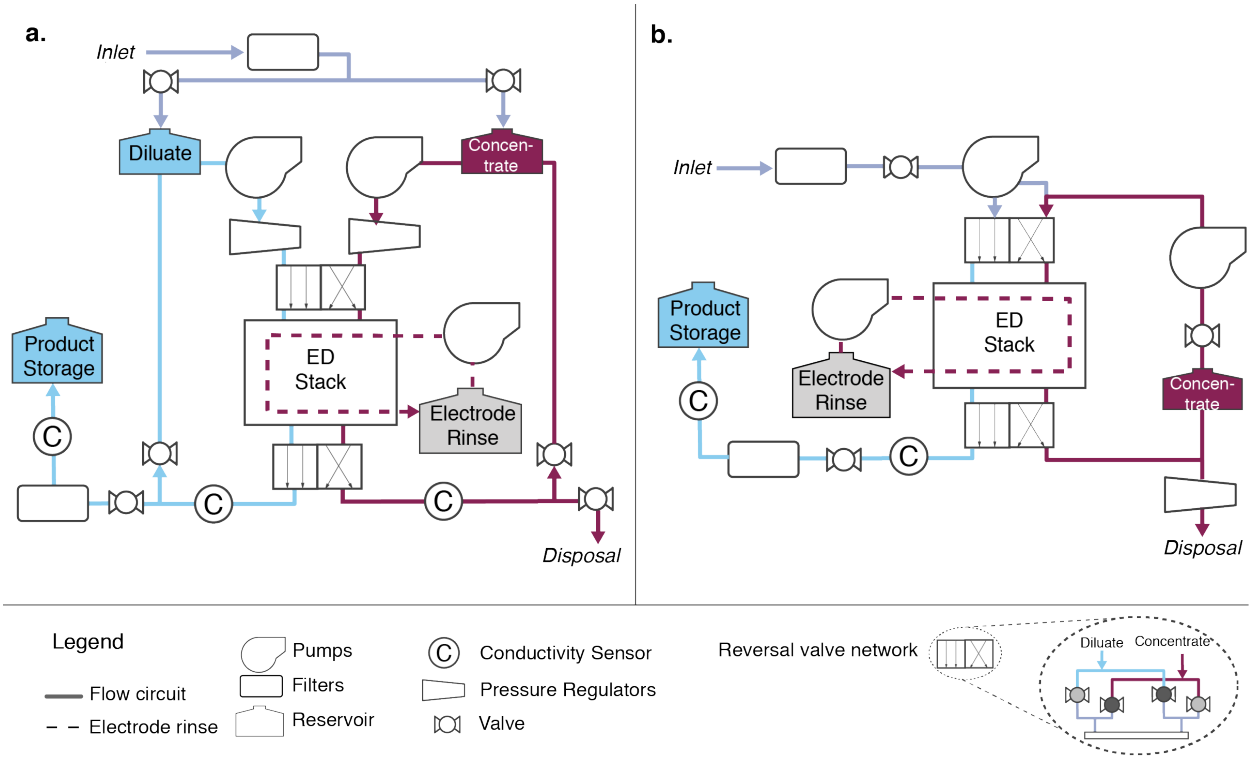


Figure 2-2: Flow diagrams of conventional batch and continuous ED architectures. Associated pump, valves, and storage tank for the acid-based scale mitigation system are not depicted. **a.** Flow schematic of a conventional batch ED architecture. Two pumps control the bulk water flow and overall recovery of the system while a third pump is required for the electrode rinse. **b.** Flow schematic of a conventional continuous feed-and-bleed architecture.

'reversal valve network' in Fig. 2-2.

The additional filtration components shown in both variants of Fig. 2-2 are required to remove contaminants other than salts from the water. Silica and biological contaminants present in the supply water can cause health impacts for users and may also cause fouling in ED systems, necessitating the same supporting filtration and purification steps present in POU RO systems [29].

### 2.3.2 Methods to increase stack desalination efficiency

For a given amount of membrane area ($LWN$) the rate of desalination (the left-hand side of Eq. 2.3), is maximized when the current density is as high as possible. However, given that $C_d^b$ is not uniform over the length of the flow path, $i$ everywhere is limited by the $i_{lim}$

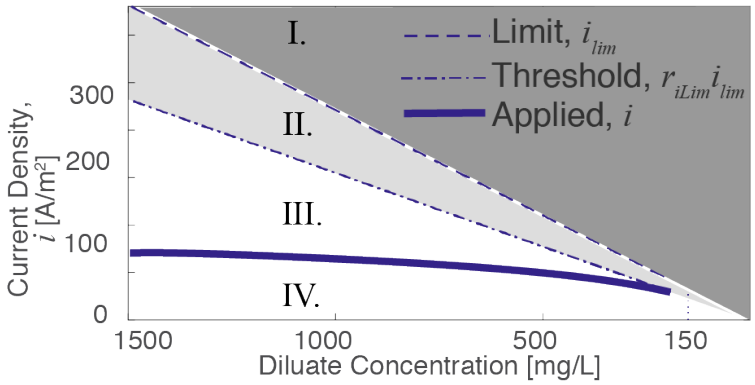


Figure 2-3: Current densities of interest over the course of a desalination process starting at 1500 mg/L and ending at 150 mg/L TDS. For a single pass through the ED stack, the limiting current density (and corresponding 0.7 safety factor threshold) decrease in the diluate stream. The maximum current that can pass through a stack can be seen to be limited by the region of lowest diluate concentration, occurring at the end of the flow path. Region I is masked given that $i_{lim}$ is exceeded in this region.

at the end of the flow path where bulk concentration is the lowest (Fig. 2-3). Region I of Fig. 2-3, above $i_{lim}$, falls outside of the operational limits of the system due to the water splitting phenomenon discussed above. By imposing a safety threshold $r_{iLim}$, we also prevent operation in Region II. The solid line represents desalination at a constant voltage, $V$. This voltage is therefore limited by the maximum applied current at the lowest concentration of the stage. This imposed limit results in a large amount of wasted desalination potential (Fig. 2-3 Region III) where the concentration could enable higher currents to be applied. Higher applied current density is desirable because it results in more efficient use of the ion exchange material, driving material needs lower and material costs down.

Two procedures can be implemented to ensure efficient use of the available membrane area in light of how the concentration limits the applied current.

While not depicted in Figs. 2-2a or 2-2b, both system architectures assume active *control* of current (often implemented via voltage control) to accommodate changes in the input feed salinity. This is necessary in the continuous system in order to remain below the current limit threshold as the feed salinity decreases (per Eq. 2.4). When current control is implemented in a batch configuration, it can be used to respond to feed salinity changes but may also be

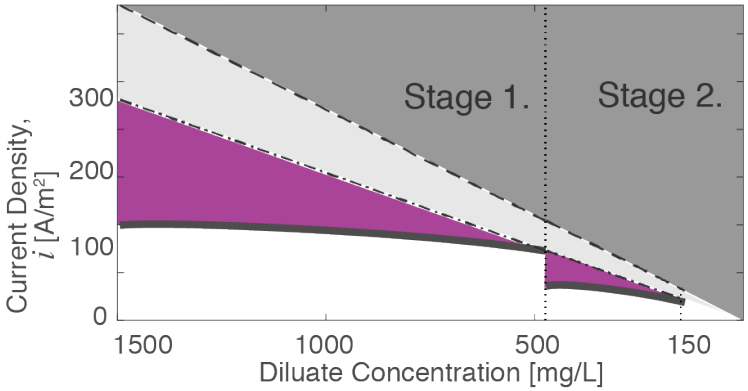


Figure 2-4: Adding two stages with independently controlled voltages minimizes the shaded region of wasted capacity by allowing the system to achieve higher desalination without reaching the limiting applied current density.

leveraged to dynamically update the applied potential over the course of a batch. Operating in this way for POU-scale batch ED systems has been shown to decrease both the batch time and required membrane area [30].

*Staging* individual stacks in series is an additional method that industrial ED systems use to adapt to feed variations by allowing more granular control of the desalination rate throughout the process of salt removal. It can be seen in Fig. 2-4 that the area of Region IV is increased by the addition of a second stage. This achieves the goal described above of operating with the applied current closer to $i_{lim}$ as a way to increase efficiency.

Staging of continuous systems allows for a standardized stack design (geometry and cell pair count) to be used in repeating units. Flow rate or current may be controlled independently at each stage to prevent the system from exceeding limiting current while still achieving a target salinity [13, 19, 31, 32]. Hybridization of ED has also been proposed in conjunction with RO by Thampy et al. [15] so that the ED system can operate at high efficiency in the first stage (maintaining high limiting currents) and water rejection is reduced at the second, RO, stage.

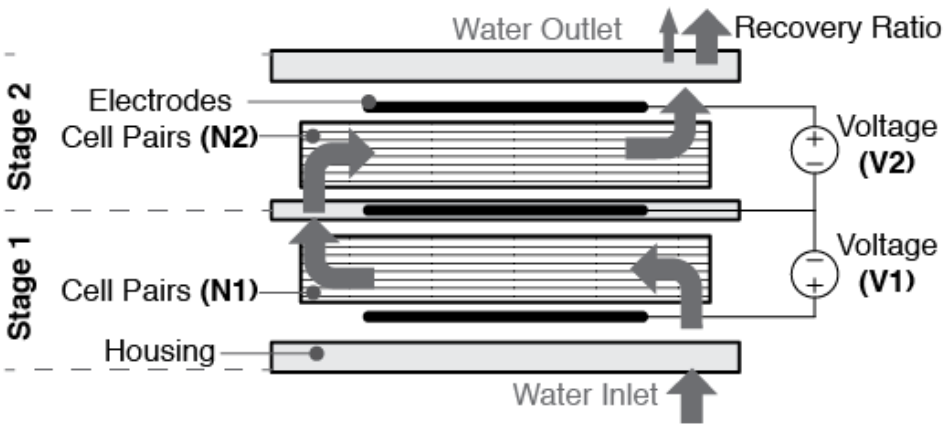


Figure 2-5: Sharing the center electrode in a 2-stage stack reduces capital cost of the system. The water flow direction is mirrored from the first to the second stage. Bold items (N1, N2, V1, V2) are variable parameters of the system.

### 2.3.3 Cost-efficient 2-stage design insight

An additional strategy to reduce capital cost is proposed through a sharing of the center electrode between both hydraulic stages of the design (Fig. 2-5). Different field strengths can be applied to each hydraulic stage using the two electrodes at the ends of the stack. Within each stage, the number of cell pairs $N$ are further allowed to vary between the two stages, therefore allowing for different flow channel velocities in each hydraulic stage. However, the length of the water flow path, $L$, and the channel width, $W$, (Fig. 4-3) are held constant to decrease the number of different components in the assembly. The shape of the flow path seen in Fig. 4-3 is made possible through the addition of a flow spacer that includes gasket area to prevent water flow outside of the specified region.

## 2.4 Parametric model-based design insights

When examined for domestic scale systems, the parametric models and understanding of system configurations produce insights and directions for further exploration of ED design that are unique from industrial-scale configurations.

*Reduced pressure drop allows for smaller pumps and less expensive components*: Due

in large part to the lower volumetric flow rate requirement (15 L/h vs >100 L/h [33]), the pressure drop decreases with the reduction of $Q_p$ in POU ED. In Eq. 2.10, flow rate is directly proportional to volumetric flow rate; however, pressure is proportional to $u_v^2$ and therefore experiences a proportionately greater change than $u_v$ as the flow rate decreases. While this effect may be somewhat counteracted by changes in channel width and length, which are inversely proportional to $u_v$ by Eq. 2.10, POU ED systems can have linear flow velocities of <50% that of industrial systems (e.g. 5 vs 10 cm/s) while still meeting the performance targets. This lower pressure drop enables smaller feed pumps to be used to operate the system as the inlet pressure required for the feed water is lower. Smaller pumps provide significant cost savings in the system.

*Shorter flow channel span allows for differential pressure to be tolerated between diluate and concentrate channels*: With the reduced pressure drop, the structural integrity of the membranes has a larger safety margin from a deflection that may cause damage in the system. Combining this with the reduced unsupported span length ($W$) of smaller geometry flow paths and Eq. 2.14 we can see that IEMs may better tolerate a pressure differential between the diluate and concentrate channels. While industrial systems devote significant effort to balance pressure between the channels, a POU ED system does not warrant the same concern.

*Recovery ratio control can be simplified by operating with differential channel flow rates*: With the ability to tolerate different pressure drops in the channels, POU ED is further able to leverage the previous insight to purposely imbalance *flow* between the channels. Intentionally regulating the system to promote differential flow rates between channels allows for the system recovery ratio to be controlled through pressure regulation on the concentrate stream and eliminates the complexity of volume control that is present in industrial systems.

*Channel height can be reduced*: To increase the desalination potential of the stack, it is necessary to increase limiting current density (Eq. 2.4). From Eq.s 2.9 and 2.5, it can be seen that $i_{lim} \propto 1/d_h$ via the mass transport coefficient. Reducing the spacer thickness therefore

increases the limiting current while also reducing the total desalination power as well by reducing channel resistance (Eq. 2.2). However, this variable is not frequently manipulated in industrial systems because pressure drop is extremely sensitive to channel height as well (related as $\Delta P \propto 1/h^3$). The reduction in pressure drop through the stack provides design flexibility to decrease the channel height and increase desalination efficiency.

## 2.5 Novel POU ED system design

From the design insights of Section 2.4, we propose an additional continuous system architecture that leverages the specific size scale of the system under consideration here. Independent control of the separate water streams is eliminated, and a single pump is proposed to power flow in the whole system (Fig. 2-6). A pressure regulator on the concentrate stream enables a recovery ratio >50% by using back pressure on the system to slow concentrate flow. This is in stark contrast to the pressure regulators used on industrial ED systems, where regulation is applied to *equalize* flow rates between the diluate and concentrate stream. This novel flow rate regulation and architecture generally are enabled by the slower flow rates, overall lower pressure drops, and tolerance for differential pressure that are unique to POU ED.

The proposed simplified ED system in Fig. 2-6 reduces component count and system complexity compared to those in Fig. 2-2, and responds to the design requirements for a low capital cost system that efficiently uses available volume within a purifier housing. As with previously discussed systems, voltage control remains a required piece of feedback control in order to accommodate variations in feed water salinity. We revisit the manufacturability and ability of the pressure regulator to maintain a stable recovery ratio in the Results and Discussion chapter.

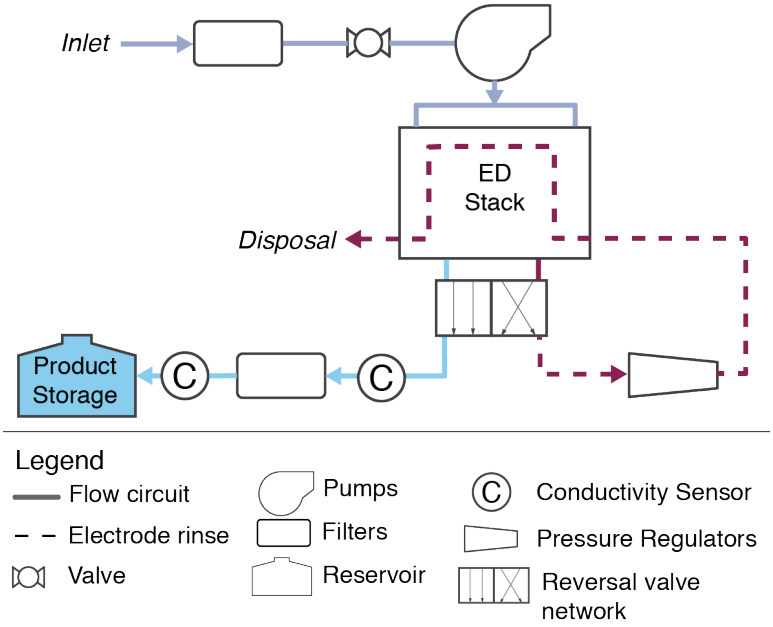


Figure 2-6: Novel *direct-flow* continuous POU ED architecture. This 'direct-flow' continuous design recycles the concentrate stream as the electrolyte and controls recovery ratio with a flow reducer.

# Chapter 3

# Two-stage prototype validation

## 3.1 Prototype design and fabrication

The purpose of this prototype was to validate the proposed 2-stage design architecture with a common center electrode (Fig. 2-5) and pressure regulator controlled recovery ratio with different flow rates between concentrate and diluate channels. We chose to validate the 2-stage variant of Fig. 2-6 prior to the 1-stage architecture as it covered validation of all aspects of the unique architecture as we envisioned them. The design parameters used for this system are listed in Table 3.1. Note that it was not built with the cost optimal cell pair arrangement in the first stage. However, for the number of cell pairs selected for the first stage, $N1$ was targeted to reduce material cost while maximizing desalination potential. The flow path dimensions are the same in both the first and second stages.

The full stack construction can be seen in the exploded CAD view of Fig. 3-1 and the photo of Fig. 3-2. The CAD depiction shows how the serpentine flow paths join at the central electrode chamber in order to transition between the two stages without flowing into the electrode compartment. The central electrode is surrounded by a manifold that was laser cut to match the dimensions of the electrode. The exposed portion of the electrode (where the exterior electrical connections are made) is sealed off from the internal electrolyte by

Table 3.1: Configuration of prototype 1-stage direct-flow continuous system

| Metric | Unit | Value | Material (Supplier) |
|---|---|---|---|
| | | *Configuration* | |
| Valves | - | 4 | 24VDC Solenoid (Malida) |
| Pumps | - | 1 | Feed pump only. FLO-2401 (Singflo) |
| | | *Spacer Mesh Properties* | |
| Thickness | [$\mu$m] | 360 $\pm$17 | Woven Nylon WN400 (Industrial Netting) |
| Void fraction | - | 65% | |
| Area porosity | - | 43% | |
| | | *Flow Channel Properties* | |
| Cell Pairs Stage 1 ($N1$) | - | 10 | - |
| Cell Pairs Stage 2 ($N2$) | - | 9 | - |
| Dimensions | [m] | 0.02 x 0.42 | |
| Total IEM area | [$m^2$] | 0.46 | - |
| Linear velocity Stage 1 | [$\frac{cm}{s}$] | 9.2 | - |
| Linear velocity Stage 2 | [$\frac{cm}{s}$] | 8.3 | - |
| Pressure drop | [kPa] | 180 | Eq. 2.11 |
| | | *Ion Exchange Properties* | |
| AEM resistance | [$\Omega cm^2$] | 30 [34] | AR204SZRA (SUEZ) |
| CEM resistance | [$\Omega cm^2$] | 30 [34] | CR67HMR (SUEZ) |
| Electrode area | [$cm^2$] | 98 | Ru-Ir coated Ti (Baoji Highstar Metals Trading Co) |

silicone in the electrode mesh and between the manifold and electrode edges.

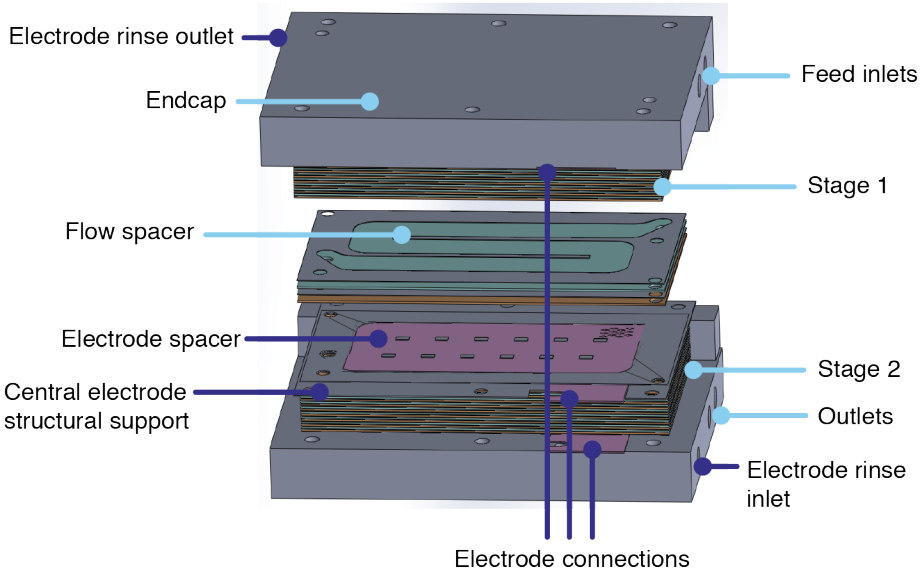


Figure 3-1: Exploded view of 2-Stage prototype.

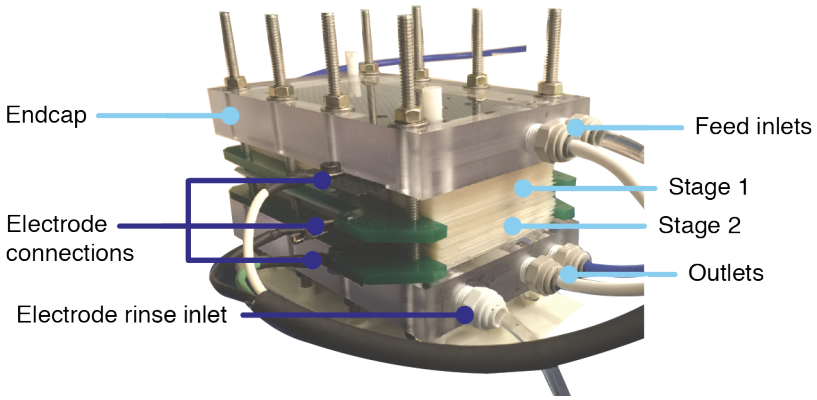


Figure 3-2: 2-Stage prototype under test demonstrating electrical connections to three separate electrodes. The edge braces are included in order to reduce slippage of the cell pairs to the side (buckling) as increased clamping pressure is applied to the stack.

### 3.1.1 Two-stage prototype fabrication

Much of the 2-stage prototype was fabricated in house. The structural endcaps were milled from polycarbonate and the central manifold was laser cut delrin, measured to the required thickness. The titanium electrodes were manufactured by Baoji Highstar Metals Trading Co per design documents provided to the company.

The flow spacers used in the prototype were manufactured using UV 60-7111 epoxy from Epoxies, Etc (Cranston, USA). Custom fabricated spacers allowed the researchers full control over the shape of the flow path and the type of mesh used in the design, which was required to determine the minimum capital cost design. The flow paths were patterned on to the spacers using an opaque vinyl pattern applied to a transparent film (Fig. 3-3). The mesh was laser cut to size then flooded with epoxy and the transparency was applied as a contact mask to the mesh. Having the mask in contact with the mesh helped ensure uniform thickness and allowed for air to be forced from the epoxy before curing. The spacer was cured under a UV-C wavelength light then excess epoxy was cleaned from the open area before a final post cure in the UV-C chamber. The variability in spacer thickness after manufacturing is captured in Table 3.1 at $360 \pm 17 \mu$m.

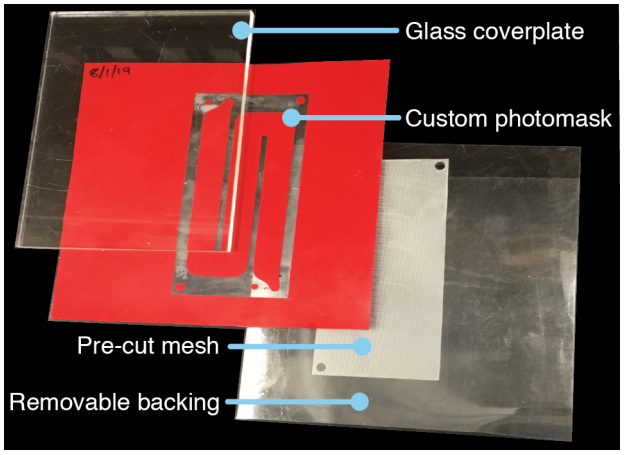


Figure 3-3: Spacer fabrication process components include a photomask of the design to pattern and pre-cut mesh. The glass coverplate is applied during the UV cure to enhance flatness of the spacer.

## 3.2 Two-stage prototype experimental results and discussion

The prototype system was tested first in Cambridge at MIT and then in Bangalore, India at Eureka Forbes Ltd.

### 3.2.1 Experimental set up and procedure

When tested in the GEAR Lab, NaCl was mixed with distilled water. This was used in order to simplify model correlations.

The field site visit took place from August $26^{th}$-$30^{th}$, 2019. The prototype 2-stage continuous system used tap water from the Eureka Forbes facility (TDS ≈1620 mg/L) as well as dilutions and concentrations of this water. This water was reported by Eureka Forbes to have a cation content of approximately one third calcium ($Ca^{2+}$). This increased 'hardness' of the test water compared to that used in the laboratory tested would be expected to have greater salt *ion* reduction for an equal amount of *charge* (current) applied to the system given the valency of $z = 2$.

In order to characterize the system, multiple assessments of the limiting current were run

for salinities ranging from 550 mg/L TDS to 1980 mg/L TDS. The limiting current point was noted visually by sweeping through increasing levels of applied voltage and observing when the current plateaued. This process was performed for the first stage with the second stage off, then performed for the second stage with the first stage operating at limiting current.

### 3.2.2 Desalination performance

The system was able to desalinate 500-2000 mg/L TDS inputs successfully to 90% TDS from 500 to 1500 mg/L TDS input feed. However, as can be seen in Fig. 3-4, the salt reduction was achieved after the limiting current was attained by the stack. The data presented in Fig. 3-4 are for a single direction of current flow withing the stack, as the performance was observed to be over 15% better in the shown configuration (90% salt cut vs 75% salt cut achievable).

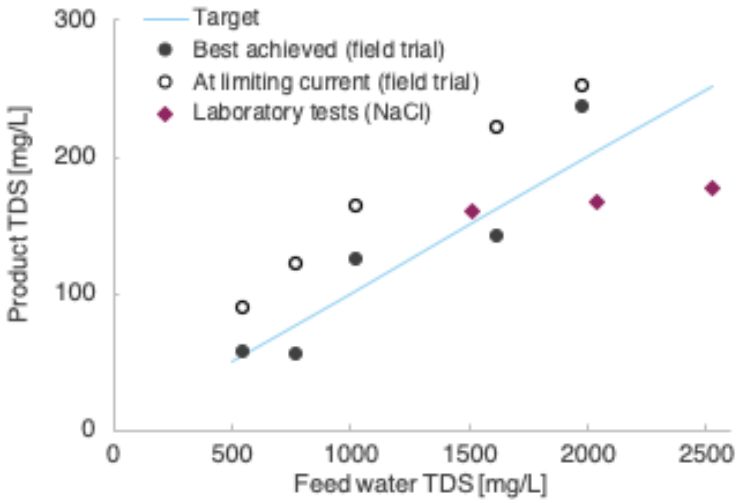


Figure 3-4: 2-Stage direct-flow continuous prototype performance. All trials were performed at 12±0.5 L/h with a recovery ratio of 0.75. The ion content was made up as specified in the legend.

Additionally, the voltages needed to achieve this desalination were higher than those predicted by the theoretical model. Three hypotheses may explain the voltage increase:

1. deviation from the empirical relation assumed for the Sherwood number that governs

mass transport and mixing within the channels,

2. membrane resistances that are higher than predicted by the model, particularly given the additional carbonate ions present in the water as compared to the lab testing as this is know to increase membrane resistance [34], or

3. other factors in the design of the prototype that caused unreliable flow of electrolyte in the electrode compartments and high resistances as a result.

Considering the final item, it was observed during testing that efforts to reduce water leakage from flow channels to the membrane edges negatively impacted the flow of electrolyte into the electrode chamber. Namely, increasing the clamping force between the two endcaps would lead to the electrolyte inlets collapsing, because these inlets were designed as voids within the mesh and therefore had no internal support from the mesh weave. The clear endcaps allowed visual inspection of the exterior two electrolyte chambers and the observation that very little water flow could take place unless the clamping pressure was reduced.

The lack of electrolyte flow not only increased the electrical resistance (and therefore power requirements) in the system, it also made the electrode susceptible to mineral scale precipitation. In addition to the low flow rate, the alkalinization taking place at the anode created conditions in the mineral-rich water to generate visually noticeable 'chalking' on the electrode. Figure 3-5 shows mineral deposits in four locations proximal to the electrode. Though this was washed off easily without needing to use acid, this observation is concerning for longer operation and reiterates the necessity of including scale mitigation strategies in a commercially-viable product for POU filters using similar quality water.

### 3.2.3 Architecture validation

The field-validation of the prototype using real water in India is an extremely promising step towards implementing POU ED in the urban Indian marketplace. Recovery ratio could be controlled over multiple days of testing to over 80%.

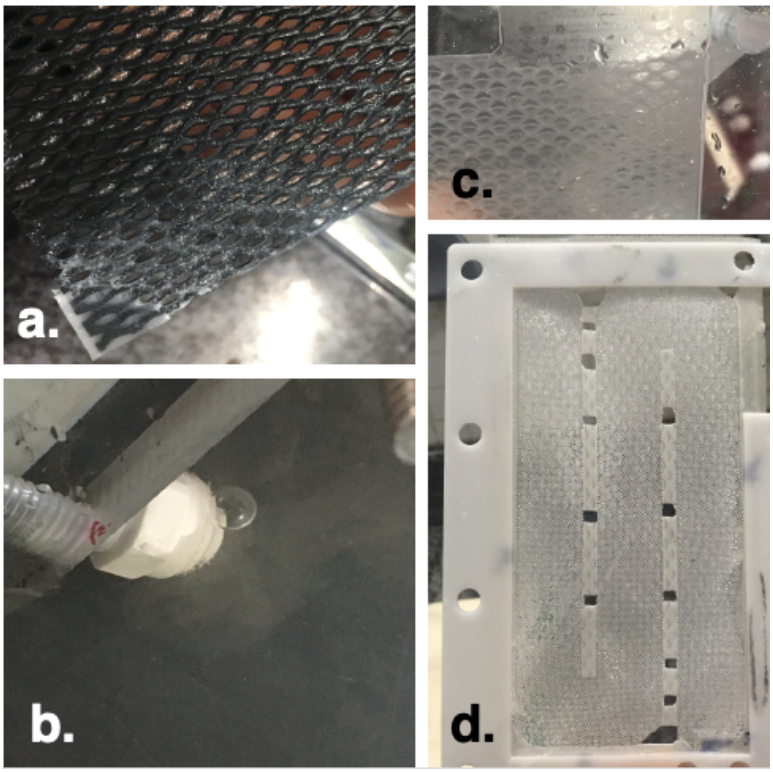


Figure 3-5: Mineral scale within 2-stage prototype. a. Scale is visible as white chalk on the electrode itself. b. The electrolyte outlet from the stack is semi-opaque. c. The polycarbonate endcap shows the pattern of the electrode, as scale formed around it, and mineral deposits leading to the outlet port in the upper right. d. the mesh spacer within the electrode component is white with minerals.

The central electrode successfully functioned as both a cathode and an anode and enabled desalination in both positions. The discrepancy observed in deslaination ability between the two positions was, however, likely a cause of the fabrication tolerances and practices used in the integration of the central electrode. The desalination results indicate superior performance of the system when the central electrode compartment was next in sequence to a concentrate channel on either side. This indicates that leakage between the first proximal channel and the electrode compartment seems likely in this design.

To enable this architecture on a commercial scale, a redesign of the 'baffle' that redistributes flow and electrolyte from the first to the second stage would be necessary.

THIS PAGE INTENTIONALLY LEFT BLANK

# Chapter 4

# System architecture comparison for POU ED

In order to determine the ED architecture that is best suited for the design requirements listed in Table 1.1, we aimed to produce an analysis that could assess the performance and feasibility of various candidate POU ED architectures, while at the same time using a unified set of assumptions and inputs. To evaluate the systems, we first perform a design study on each stack to determine the capital-cost optimal configuration, then we evaluate each cost-optimal design against the manufacturing and installation requirements of Table 1.1 and the other candidate systems.

## 4.1 Considered system architectures

The systems compared were: 1) a batch system per Fig. 2-2a; 2) a 1-stage direct-flow continuous system per Fig. 2-6; and 3) a 2-stage direct-flow continuous system as described in Chapter 3. The 2-stage system analyzed utilizes a shared central electrode as proposed previously by the authors [32]. The selection of these systems was guided by the objective to minimize capital cost while also surveying a broad range of architecture options. Direct-flow style continuous systems (Fig. 2-6) were considered instead of a feed-and-bleed style system

(Fig. 2-2) given the design insights of Section 2.4 indicate operating a POU ED stack in this manner is feasible, and the architecture's lower part count will lead to smaller packaging volume and lower cost than feed-and-bleed architectures.

### 4.1.1 Mineral scale mitigation

In all the system architectures studied, mineral scale mitigation was achieved through the inclusion of a subsystem that would store and dose acid into the concentrate stream during operation. This is particularly important in the direct-flow continuous systems where the slow concentrate flow rate causes increased residence times and may result in nucleation of precipitates. The amount of acid required was determined by using the Langelier Saturation Index (LSI) method and standard synthetic groundwater composition profiles for India containing calcium and magnesium carbonate [16]. By predicting the saturation pH at which carbonate will precipitate in the water, the LSI provides a measure of how likely carbonate scale is to form.

Acidifying the feed water reduces the LSI to bring it within acceptable limits. An LSI up to 1.8 has been recommended for industrial ED systems [19]. We chose to apply a more conservative threshold of 1.4 in the POU devices considered here. The acid storage volume in the system was calculated to reflect the volume of 3 molar citric acid required to maintain the concentrate feed volume below an LSI of 1.4 for six months of operation. The service interval was chosen based on Table 1.1 and citric acid was selected over stronger acids such as HCl given the requirement for consumer safety and the in-home application. As a result of being linked to the ion concentration in the concentrate flow, the acid requirement varies significantly with the recovery ratio of the system.

Fig. 4-1 provides the estimated volume requirements for citric acid required in a year to achieve LSI threshold mapped over input salinity and recovery. Significant reduction in the acid requirement is achieved by marginal reductions in the water recovery. For the salinities examined in the trade-off analysis, 0.6 L, 1.0 L and 2.5L per six months of operation were

required, resulting in cost estimates of \$0.1, \$2.1 and \$5.1 USD for annual acid cleaning requirements to be met.

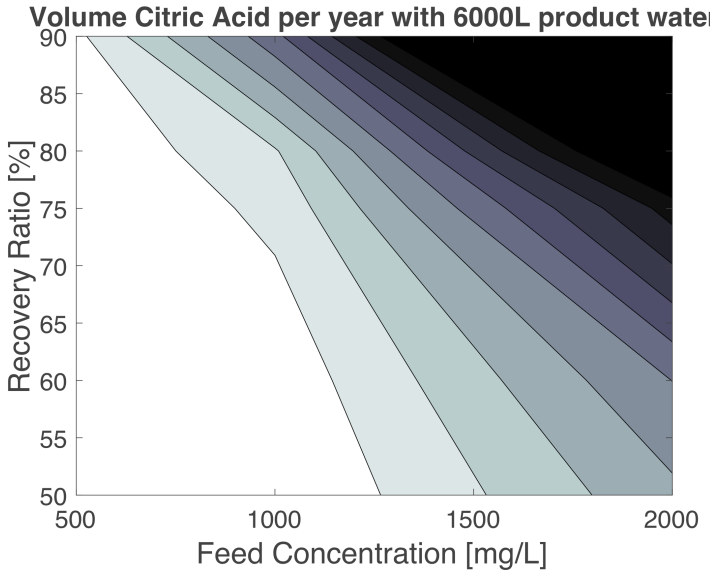


Figure 4-1: Citric acid required as a function of recovery ratio and feed salinity. the darkest region is volumes over 2 L per year whereas the unshaded region does not require any acid addition to mitigate scaling of calcium carbonate per the LSI threshold assessment.

## 4.2 Cost modeling

Examining the sub-components of our objective equation for cost (Eq. 1.1) in detail, we see that $CC_{\text{filtration}}$ and $CC_{\text{scale mitigation}}$ are fixed across any POU ED system designed for the same feed water. For the following analysis, the filtration costs $CC_{\text{filtration}}$ was set to \$47 as determined from publicly available component replacement costs described in Appendix B.

The cost of the hydraulic network $CC_{\text{hydraulic,electrical}}$ includes the pumps and valves required to operate a given architecture as well as the number of ED control systems. Table 4.1 summarizes these main hydraulic components. The unit cost estimates listed are based on currently available market data (see Appendix B for full details). The counts for pumps and SVs include all the valves and pumps required in a purifier using ED desalination. The reservoirs are unique additions in the ED system and do not include the product storage

tank. Similarly, the cost of the electronics is solely for the additional voltage regulation and stack control necessary in ED.

Table 4.1: Comparison of batch and direct-flow continuous systems on the basis of hydraulic part count. Pump and SV counts are inclusive of all components in the system while other lines represent only the items required to replace the RO module of existing POU purifiers. Cost sourcing available in Appendix B when not specified.

| | Unit Cost [US$] | Part Count | | |
|---|---|---|---|---|
| | | Batch | Continuous | |
| | | | *1-stage* | *2-stage* |
| SV | 2.5 | 11 | 7 | 11 |
| Pump | 16 | 3 | 2 | 2 |
| Electronics | 2 | 1 | 1 | 2 |
| Reservoir | 2.5 | 3 | 1 | 1 |
| Flow Baffle | 4 | 0 | 0 | 1 |

With all the previous costs set by the architecture, $CC_{\text{ED stack}}$ is the only component cost that can be truly minimized in an optimization. The capital cost of a stack is determined by the structural components and the area of IEM and electrode required to achieve the desalination target. The structural costs were here assumed to be constant across all POU ED designs given they make up a small fraction of the stack cost. By contrast, the electrodes and IEMs are priced on a per-area basis as 2000\$/m$^2$ for the electrodes [35], 40\$/m$^2$ for the IEMs [36], and 0.06\$/m$^2$ for the spacers (see Appendix B for further details).

## 4.3 Optimization problem definition

In order to compare the architectures described, we set out to determine the capital cost optimal configuration of each design through a constrained optimization. The performance of each design was then compared to the qualitative design requirements determined previously.

The *objective* in all instances was the capital cost, as calculated per the previous section. The design parameters of Table 1.1 ($Q_p = 15$ L/h, $r = 0.9$, salinity reduction of 90% from feed, pH = 7.8) were input into the parametric models for both batch and continuous systems.

In order to handle the range of feed salinities presented in the requirements, we chose to discretize the search space and determine cost optimal designs for feeds of 500, 1500, and 2500 mg/L TDS. This allowed us to quantify the effect of feeds variation on the configuration and cost of the resulting designs. Further, we chose to approximate the full TDS as being derived from NaCl. This approximation has been used previously by Wright et al. [21], where it was shown to provide accurate predictions of the experimentally measured desalination rate and SEC within 20% and 22%, respectively.

The same membrane and spacer material properties were used across all the analyses in the optimization. The parameters (shown in Table 4.2) are based on those seen in the commercially available PCCell GMBH (Heusweiler, Germany) bench-top ED unit. The membrane resistances are based on experimental results from Ortiz et al. [22] for comparable Neosepta ion exchange membranes, scaled to 1.3 times their result given the findings of Moe et al. [34], which reported resistance of membranes in groundwater can be higher even than that predicted using NaCl measurements. A further sensitivity to mesh parameters can be seen in Appendix 4.5.2 as well.

Table 4.2: Modeling parameters used in calculated predicted system operation during optimization studies. Parameters are based on commercially available materials for ED systems intended for laboratory-scale applications.

| Metric | Units | Value |
|---|---|---|
| *Spacer Mesh Properties* | | |
| Thickness | $[\mu m]$ | 350 |
| Void Fraction | - | 0.62 |
| Area Porosity | - | 0.6 |
| *Electrical Properties* | | |
| AEM Resistance | $[\Omega cm^2]$ | 40 |
| CEM Resistance | $[\Omega cm^2]$ | 40 |

The search space included length and width of the flow path ($L$ and $W$) as well as number of cell pairs ($N$) as *decision variables* that were varied throughout the solution process. *Hard* (inflexible) constraints were placed on $V_{max}$, system volume, $P_{max}$ and recovery ratio ($r$)

based on the limits of Table 1.1. A sensitivity analysis to $V_{max}$ was performed to ensure that the limit was not over-constraining the design space and eliminating possible better alternatives (see Appendix 4.5.2). A further limit was placed on the design optimization by constraining the system to operate with a margin of safety below the limiting applied current. Industrial best practice is to maintain operation such that the applied current stays below 70% of $i_{lim}$ ($r_{iLim} = 0.7$) [12, 31].

### 4.3.1 Batch system optimization procedure

The total IEM and electrode areas in the batch system were calculated based on the theory outlined in Section 2.2 combined with the previously validated cost-optimization proposals for batch POU ED by Wright and Shah in [21, 30]. In their 2019 work [30], Shah et al. expand Eq. 2.3 to a relation between the feed and product salinity as

$$\frac{V_{dil}}{t_{batch}} \ln\left(\frac{C_{feed}}{C_{prod}}\right) = \frac{LWN\overline{r}\phi k}{1 - t_{+,-}}. \tag{4.1}$$

Here $\overline{r}$ is a time averaged recovery and the batch time ($t_{batch}$) is related directly to the salt reduction.

The authors had previously previously proposed and validated a POU batch ED design in [20]. Combining the previously proposed optimal batch design with the scaling relation described by Eq. 4.1, we were able to re-size the $LWN$ of the optimal system that was initially proposed based on the design requirements $C_{feed}$, $C_{prod}$, $Q_p = V_{dil}/t_{batch}$ and $\overline{r}$ of Table 1.1 and the mesh parameters of Table 4.2. Additionally, the operation of the batch system was made representative of in-service operation by requiring 25% shorter batch times than simply predicted by the volumetric flow rate requirement, in order to allow for the down time required to flush the ED unit between batches.

### 4.3.2 Continuous system optimization procedure

For the continuous type system architectures, the desalination over a given membrane area and flow geometry was calculated by discretizing the flow path length, $L$, and numerically solving the system of equations as proposed in [21] to determine the incremental reduction in bulk concentration over the length of the flow path. This transforms Eq. 2.3 into a boundary value problem where the flow path geometry and number of cell pairs can be manipulated to obtain the required salinity output $C_d|_{x=L} = C_{prod}$. A full system model that also accounted for the secondary mass diffusion effects of osmosis and back diffusion was used in the "Model Seek" step of Fig. 4-2 to produce designs for a linearly incremented number of cell pairs until a minimum was obtained. This was repeated for flow path widths of half-centimeter increments and the capital cost of the resulting designs at each width were compared manually to determine the final cost-optimal design.

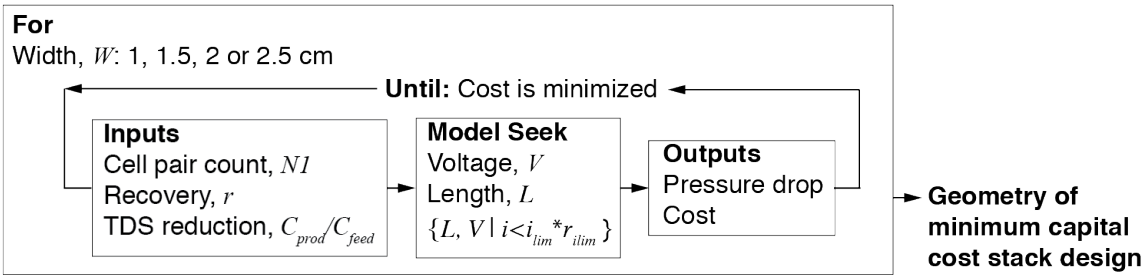


Figure 4-2: Optimization of 1-stage direct-flow continuous stack was performed using an iterative process.

A similar optimization process was used for determining the capital cost optimal 2-stage stack designs, with the added dimension of allowing the number of cell pairs and applied voltage to change independently between the two stages. Further details of how the process was executed, including how the ratio of desalination between the first and second stage was determined, can be found in the author's previous work [32].

In both system designs (batch and direct-flow continuous), the cost of the IEM was a combination of the active IEM area determined from the models and a width of gasket outside the edges of the channel to seal the channels (Fig. 4-3. The cost of the IEM was

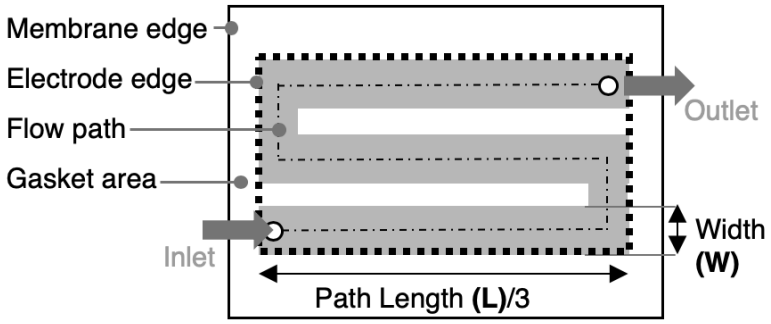


Figure 4-3: Within a single cell pair, the flow path is torturous in order to conserve area. The membrane and spacer have the same outer edge but the electrode is only required in the area of water flow.

the total area multiplied by the unit cost. The flow path was 'wrapped' back on itself for a final area of $A = (\frac{L}{3} + 2t_{gasket})(3W + 4t_{gasket})(CC_{\text{per area}})$. The gasket of the batch systems was wider (1.2 cm) than that used in the continuous system estimates (0.8 cm) given the high pressures of the batch systems. The gasket width of the batch system was measured from the commercially available bench-top PCCell unit that was also used as the basis for the mesh parameters.

### 4.3.3 Two-stage optimization procedure

In identifying the cost-optimal two-stage system, we focused on the variable cost materials (membranes and electrodes) to drive my analysis. The fixed costs were added after the minimum cost design based on electrode and membrane cost was established. Analysis by Nayar et al. [13] predict that 91% of the module cost is due to ion exchange membrane and electrode costs alone, therefore these were the two costs considered in estimating capital costs in this analysis. Total area of the membrane and electrode was calculated from the specified flow path $L$ and $W$ plus additional material around the path that gasket to prevent water leaking from the channel (Fig. 4-3).

The minimum capital cost design was determined through a scatter search. In structuring the simulations, geometric properties of the path were varied through specified ranges and the model described above was used to calculate the voltage required in each stage to achieve

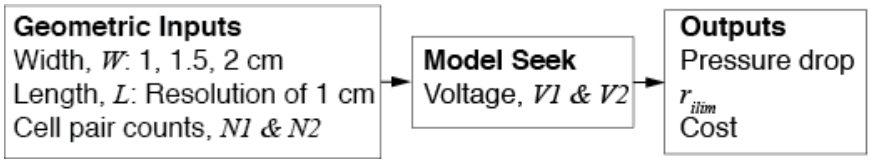


Figure 4-4: Geometric inputs are selected over a range of inputs and fed to the computational model that returns system characteristics of interests for each design. Width was resolved at 0.5 cm from 1.5 to 2.5 cm; length was resolved at 1 cm; N1 was assessed from 8 to 22 cell pairs; N2 from 6 to 11 cell pairs for N1=13 and rescaled as necessary for N1 values at extremes of the range.

the desired salt reduction (Fig. 4-4). The resolution for the widths was chosen based on limitations of the fabrication process of flow spacers within the lab setting where widths have been demonstrated to be controlled within 2 mm.

The product salinity $C_{prod}$ and intermediate salinity $C_{int}$ were both specified as inputs to the model. The intermediate salinity was fixed as the geometric mean of $C_{feed}$ and $C_{prod}$ as described by Equation 4.5. This was determined analytically from methodology similar to that presented by Shah et al. [30] and modified to assess the desalination potential in a single pass through the continuous system.

Assuming the total active area required is the sum of the area in the first and second stage, the optimal intermediate concentration, $C_{int}$, can be found by taking the partial derivative of total area with respect to $C_{int}$ per Equation 4.2.

$$\frac{\partial A_{Total}}{\partial C_{int}} = \frac{\partial A_1}{\partial C_{int}} + \frac{\partial A_2}{\partial C_{int}} = 0 \tag{4.2}$$

Equation 4.3 gives an approximate ratio of feed to product concentration for any stage given a total membrane area, $A_{total} = WLN$, open area porosity of the spacer, $\phi$, threshold ratio of applied to limiting current, $r_{iLim}$, minimum of the ion transport numbers between cation and anions in the solution, $t_{+/-}$, here taken as $t_+ = 0.39$ for $Na^+$, flow rate per cell pair, $Q$, and mass transfer coefficient, $k$. Refer to Shah et al. for the assembly of these

variables into the relation used here [30].

$$\frac{C_{feed}}{C_{prod}} = 1 + \frac{\phi r_{iLim} W L N k}{Q(1 - t_{+/-})} \tag{4.3}$$

With consistent spacer material properties this simplifies to an equation relating area to the desalination ratio with a constant factor, $\mathcal{R}$, per

$$\frac{C_{feed}}{C_{prod}} - 1 = \frac{\mathcal{R} A}{\sqrt{NW}}. \tag{4.4}$$

Noting that the intermediate concentration of the full ED stack will be the product of stage 1 and the feed into stage 2, Eq. 4.2 can be used to determine the full relationship of $z$, $C_{int}$, and $C_{prod}$ as

$$C_{int} = \sqrt{C_{feed} C_{prod}}. \tag{4.5}$$

This analytical method was validated using the system simulation in Appendix A.

## 4.4 Evaluation and comparison of candidate designs

### 4.4.1 Candidate designs

Table 4.3 presents the resulting configuration and total capital cost of a batch system and a one- and two-stage direct-flow continuous system for a feed TDS of 1500 mg/L TDS NaCl. The 1500 mg/L case is presented here given it captures a larger percentage of the target market than the 500 mg/L design (96% compared to 76% per Table 1.2) while not being over-designed for the target market, and therefore more expensive, as with the 2500 mg/L case. A full comparison of the costs of the other designs can be seen in the Appendix C.

The estimated cost of the conventional batch system and a single-pass continuous system are comparable (within 5%). Purely with regard to the objective function, these designs are well matched. Table 4.3 presents the key differentiating characteristics of the batch and

continuous systems considered, namely volume, stack configuration and energy consumption. The systems align on the resulting designs for acid volume (1 L for 6 months of operation) and cost of the acid addition system, given that the requirement is based on the concentrate salinity, which is a result of the fixed recovery ratio and feed salinity.

Table 4.3: Optimized POU ED architecture comparison results highlighting key differences between the systems, including ED-specific component volume and electrode area. All were designed for feed water with 1500 mg/L TDS and required 1 L additional volume for acid.

| | | Batch | Direct Continuous | |
|---|---|---|---|---|
| | | | 1-Stage | 2-Stage |
| Capital cost | [US$] | 202 | 195 | 209 |
| Package volume | [L] | 8.5 | 5.1 | 5.8 |
| Cell pairs | - | 30 | 39 | 23 |
| Electrode area | [$cm^2$] | 86 | 115 | 109 |
| SEC | [$\frac{kWh}{m^3}$] | 1.08 | 0.35 | 0.7 |

### 4.4.2 Cost breakdown

Regarding the optimization objective, the main *cost* drivers are in the membrane and electrode cost, with the stack making up 37% of the predicted batch system cost, and 51% of the predicted 1-stage continuous system cost. When considered in a comparable breakdown to that presented in Table 4.1, the supporting electronics components are predicted to be comparable at 10% of the total system cost in both batch and 1-stage continuous systems, while the hydraulic components (pumps, valves, and reservoirs) are 37% and 19% of the cost, respectively, reflecting the added components in the batch system. The standard filtration components and main reservoir make up about 15% of the cost in both system variants. While economies of scale can vary the exact costs seen for each component, the same assumptions were used across all compared systems.

### 4.4.3 System operation adaptability and energy usage

Energy consumption, while not a constrained requirement per Table 1.1, was calculated for the candidate designs using Eqs. 2.12 and 2.13, with a pumping efficiency of 0.5. The SEC is threefold higher in the proposed batch system as compared to the direct-flow continuous system. This difference is driven in part by the higher linear flow velocity in batch systems (18 cm/s as compared to 4 cm/s) that leads to greater pressure losses and work required by the pump. We include this result as reference for researchers who may be interested in the architecture comparison in an application where this design requirement is constrained.

Responding to the initial requirement that the system must *adapt* to variations in feed water, we must compare the effect of feed salinity changes on each type of system separately. While both experience a change in performance, batch systems experience this change as a decrease or increase in batch time and therefore the production rate. By contrast, continuous systems maintain flow rate but sacrifice current density: either less efficiently applying current for lower salinity water, or exceeding limiting current in the case of a higher salinity feed in the effort to achieve the same target concentration. Considering the full range of feed salinities discussed in Table 1.1, we are also able to compare the resulting performance of each system with a wider range of salinities. Table 4.4 shows that both systems sacrifice one performance metric at a higher feed salinity. Notably, the metric being sacrificed in a batch system is the production rate, while the requirement that is not met in the continuous system is output salinity. Depending on the context of installation, either one of these requirements may be more valuable to a target customer.

Alternately, we chose to examine how the systems could handle changes in feed salinity if a temporary excursion beyond the design requirements were allowed. We did this by allowing a 10% excursion in the flow rate (for the batch systems) or limiting current safety factor (for the continuous systems), then assessing the maximum feed salinity that the system could process to 90% salt cut. In the batch system, degrading the output flow rate to 13.5 L/h resulted in a maximum feed salinity of 1938 mg/L TDS being tolerated. In the continuous

systems, increasing $r_{iLim}$ to 0.8 allowed the systems to meet the original target output of 150 mg/L with a feed salinity ≤1750 mg/L for the 1-stage design and ≤1910 mg/L for the 2-stage design.

Table 4.4: Comparison of performance changes for a system optimized for a feed salinity of 1500 mg/L when the feed salinity varies. The target output salinity is maintained at 90% or 150 mg/L, whichever is less. In both systems the current and voltages thresholds of $r_{iLim} = 0.7$ and $V_{max} = 24$ V were maintained.

| | | Feed Salinity [mg/L] | | |
|---|---|---|---|---|
| | Unit | 500 | 1500 | 2500 |
| Batch modified production rate | [L/h] | 28.7 | 15 | 12.3 |
| Continuous output salinity (1-stage) | [mg/L] | 50 | 150 | 738 |
| Continuous output salinity (2-stage) | [mg/L] | 50 | 150 | 750 |

### 4.4.4 Manufacturing and installation

When considering the additional design parameters of Table 1.1, many of the requirements are met equally by all three systems. All systems include sufficient consumer-safe citric acid to maintain LSI below the chosen scaling threshold for 6 months, the standard maintenance term of a POU RO system. Components used in the representative bill of materials cost and volume estimates were in large part chosen from commercial components already in use in POU RO systems or sold by similar manufacturers, fulfilling a second requirement on the list.

A main differentiator between the systems is the estimated *packaging volume*. The packaging volume in Table 4.3 is the volume of the stack and hydraulic components that will be added to the system. It does not include the volume needed for an acid tank, but does include the valves required for that system. Individual component volumes were estimated from measurements of the representative components used in commercial RO POU desalination systems and multiplied by the component count of Table 4.1. The volume of each part for purposes of the estimation was approximated as that of a rectangular prism 'bounding

box' that the component could fit entirely within. The over-estimate of volume for the many roughly-cylindrical components was intentional in order to account for the volume required for cable and hose routing within the system.

The batch system volume is estimated at 66% higher than the direct-flow 1-stage continuous system and double that of the 2-stage system. In a packaging constrained application this difference may dictate the overall feasibility of the system. While the estimated stack volume is comparable within 12% (2300 $cm^3$ for batch vs 2600 $cm^3$ for 1-stage direct-flow) the overall volume discrepancy between the two types is driven by the reservoirs required to store diluate and concentrate during the purification process and by the valving required to enable reversal in a batch system (64% and 39% of the predicted system volume, respectively). The 2-stage system more efficiently uses the membrane area [32], reducing the stack volume. Given the upper bound estimation of allowable system volume of 6000 $cm^3$, the cost-optimal batch system exceeds the requirement placed on the form of the system.

The direct-flow continuous systems have greater manufacturing assembly and functional similarity to POU RO systems than the batch system. The workers within the supply chain of the POU systems are most familiar with direct-flow systems. By eliminating intermediate tanks and maintaining singular points for input and output, there are fewer points of confusion and assembly errors for factory and maintenance workers.

### 4.4.5 Chosen architecture

Considering the design requirements of the Indian domestic market, the proposed 1-stage direct-flow continuous architecture is the best (and only) option to meet these constraints. By setting an upper bound feed salinity to 1500 mg/L, the system shows cost savings that outweigh the 'adaptability' benefits of batch systems. Furthermore, after incorporating the requirement for reliability, and therefore scale mitigation, the batch system is all but eliminated as a feasible design. Continuous systems have the added benefit over batch of approximately half the powered components (valves), increasing the overall reliability by decreasing

the points of electromechanical failure.

Between the 1- and 2-stage direct-flow continuous designs, the cost is within 7% and the volume is within 14% with the 1-stage design having the advantage in both criteria. While both 1- and 2-stage continuous systems exist in industrial-scale ED, to the authors' knowledge, no multi-stage system utilizes a single electrode between stages, instead requiring two electrode plates (at the same potential) on either side of a structural manifold. This added complexity for the 2-stage design proposed here has the potential to decrease reliability by adding points of failure. By contrast, if each stage had a dedicated electrode pair, the cost of the 2-stage design will increase by $22 over that predicted in Table 4.3.

## 4.5 Sensitivity of objective to constraints and design inputs

### 4.5.1 Active constraint visualization

In an effort to better understand how the constraints effected the optimal designs, I completed an additional series of visualizations. This process is presented here for the 2-stage direct flow continuous system, but can be used with a one-stage system as well given that the analysis is essentially the same given the cell pairs in the first stage were fixed for a given set of plots in the 2-stage case.

The intent was to generate a set of tools to compare the impact of different variables on the final cost, and to provide a more intuitive understanding of how geometry changes affect resulting cost-optimal designs. To begin, Fig. 4-5 can be used to connect how changes in geometry over the domain affect key outputs. For this visualization, $N1$ is fixed at 13 and $W$ is fixed at 2 cm while $L$ and $N2$ are varied. The visualization is a useful tool when considering how variations in external constraints (such as the maximum available voltage or pumping pressure) may change both the shape and cost of the ideal design.

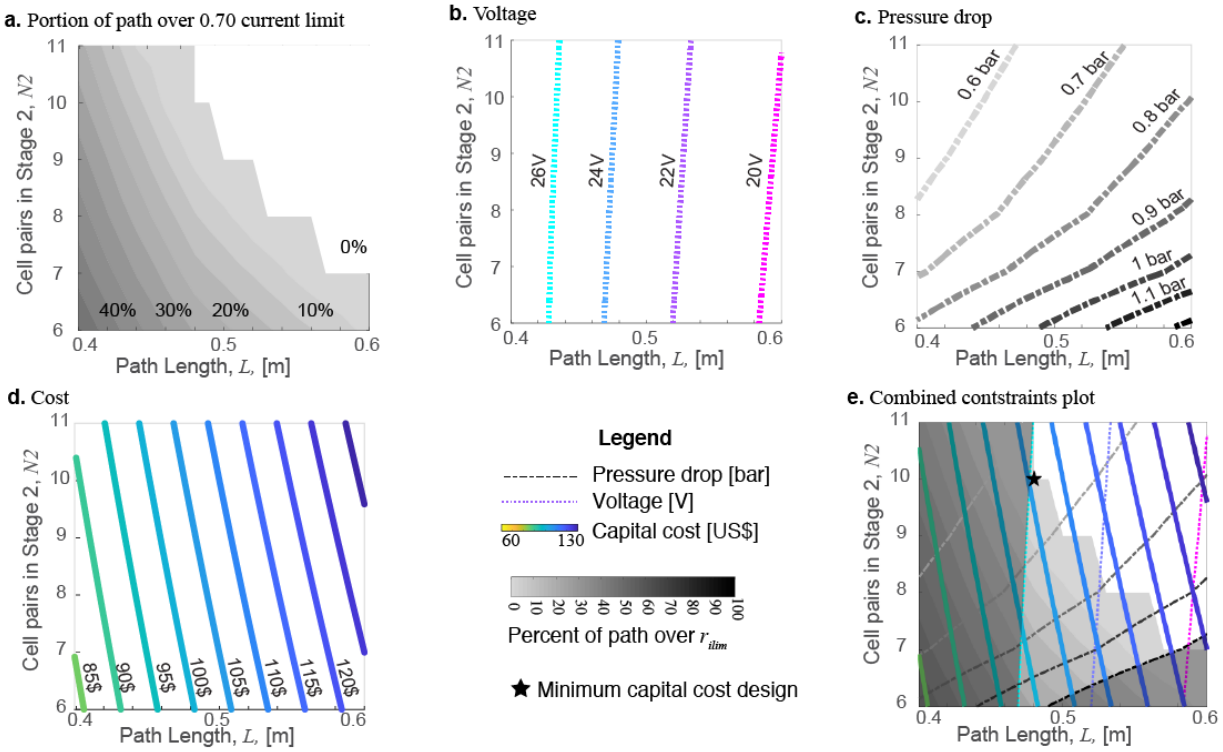


Figure 4-5: Design space exploration for a path width 20 mm, 13 cell pairs in the first stage **a**. Increasing active area decreases the percentage of the flow path over the applied current threshold **b**. Voltage decreases with lower cell pair series resistance or increased path length **c**. Pressure isobars show increasing pressure with geometric changes that increase channel flow velocity. **d**. Increasing the active area of a single cell pair has a greater effect on cost than increasing the number of cell pairs given the higher relative cost of the electrode compared to the membrane. **e**. The optimal design lies on the limiting current ratio constraint boundary. It includes 13 cell pairs in stage 1, 10 in stage 2, a path length of 0.48 m, path width of 0.02 m and results in a capital cost of USD106 for membranes and electrodes. Path width 20 mm.

The first parameter considered when exploring the design space was how the applied current density was affected by path length and cell pair counts. This is a technical constraint imposed on the system and therefore the boundary is immobile in the case of potential system improvements by the designer. Figure 4-5a shows the permissible and impermissible (shaded) regions of the design space as bounded by the constraint on $r_{iLim}$. For the same geometry, increasing the $N2$ cell pair count (moving up the vertical axis) decreases the amount of the path over $r_{iLim}$ by slowing the flow velocity. This type of system modification is possible to implement after a stack has been designed and is a notable point of flexibility.

Fig. 4-5b shows that as active area per cell pair increases with growing length, the voltage required to achieve a target concentration also decreases. This occurs because a lower corresponding applied current density is required to remove the same salt. The slight vertical increase in voltage is required to overcome the increasing resistance with more cell pairs added to the second stage.

Given the relation of pressure to $u_v$ (Equation 2.11), it is reasonable that the lines of constant pressure shown in Fig. 4-5c are sensitive to geometry changes that influence the void channel velocity and increase in proportion to longer flow paths or fewer channels. Again, a designer could modify a system design in this way in order to meet a change in the pressure constraint.

The performance of this design relative to constraints is visualized in Fig. 4-5e. The constraint limits have been overlaid onto the composite plot as shaded regions. Voltage requirements over 24V would fall to the left-hand side of the plot, nearer the y-axis. Pressure drop predictions over 1 bar fall in the lower right portion of the plot and are also excluded. The only active constraint at this optimum is $r_{iLim}$. While the predicted voltage is close to the 24V limit, the constraint is not considered active because there is no feasible solution with a lower capital cost if only the applied current constraint is considered (i.e. relaxing the 24V limit does not affect the optimal design choice).

As a point of comparison, the same process of visualization can be used on varied path

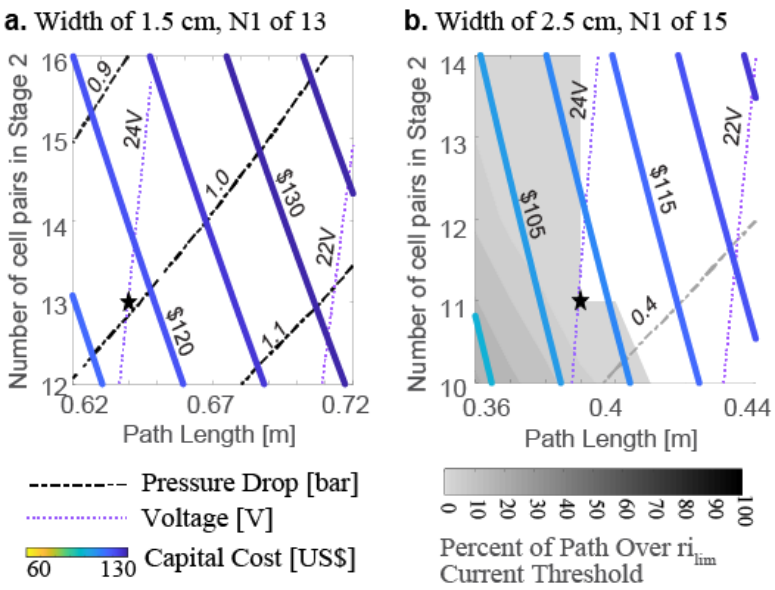


Figure 4-6: Feasible design solutions for varied path geometries. **a**. The minimum cost attainable is higher than the optimum as the design is limited by the pressure and voltage constraints. This results in more cell pairs and a greater length flow path. **b**. Shows an alternative design (with thicker flow path width) that is instead limited by the applied current threshold.

widths, $W$ to see how the active constraints at the cost-optimum point change. Pressure loss is also highly sensitive to flow path width for a given volumetric flow rate. In the case where pressure loss was known to be of concern, a wider path would be favorable to decrease this loss. Modifying the design width is a decision that would need made prior to fabrication, as it drastically changes the flow path form (length and cell pair count) so it is useful to have this parametric understanding prior to the design phase.

Here I examined what cost increase was derived from presetting the path widths 0.5 cm above and below the determined cost optimal width. Figure 4-6 shows the constraint plot of these two configurations. Of note here are the active constraints for the new design widths: pressure drop and applied voltage limit the design for the 1.5 cm path width system (Fig. 4-6a), whereas the 2.5 cm width case is limited by the current threshold (Fig. 4-6b).

When the flow path width is increased, $u_v$ decreases, therefore reducing the mixing within the channel and resulting in a lower limiting current density. In order to compensate for the lower applied current density, the total active area must increase through increasing the

cell pair count or path length. This system would operate at a lower pressure than the 2 cm width cost-optimal design, which could be favorable in a low pressure (e.g. gravity fed) application.

In considering the case of decreased width, the maximum voltage constraint is active, forcing a longer path length in order to increase the active area of the system and decrease the applied current density. Pressure drop is also proportional to path length (per Eq. 2.11), so the pressure drop constraint begins driving the addition of cell pairs in the design order to reduce the flow velocity. The capital cost of this design would be reduced if either the pressure or voltage constraints were relaxed, pointing to the potential need for a more powerful pump or voltage supply.

Access to the visual relations of active constraints portrayed in Figs. 4-5e and 4-6 allow for rapid assessment of the limiting factors in the design and where additional efforts should be focused to provide further reduction in capital cost. From this case study it is clear that for the cost-optimal design, neither the available pump or voltage supply impose a limit on cost. However, examining the height, porosity, and mixing of spacers within the stack may provide the best avenue of further development. In light of this, a more detailed sensitivity of the cost to these specific parameters can be performed.

### 4.5.2 Cost sensitivity of ideal design to input parameters

A series of sensitivity analyses were performed on the ideal architecture design for individual parameters. They were performed for the three probed input salinities but are displayed here for 1500 mg/L only for clarity. the first set of sensitives focus on the influence of mesh geometry on the final cost with the goal of aiding in the early design phases and material selection. The second set examine if the design constraints imposed on the system are eliminating possible lower-cost alternatives that would warrant a critical examination (and possibly alteration) of the constraints as they are currently defined.

### Cost sensitivity to feed salinity in continuous systems

In light of efforts within the Indian government to encourage water conservation by imposing a minimum TDS value for POU purifiers, we chose to further explore how the cost prediction for the optimal designs would be effected by a target of 80% salt reduction instead of 90% reduction as assessed in the initial design. Holding the remaining variables described in Section 4.3 constant, we relaxed the target output salinity to 300 mg/L and optimized for capital cost within the new set of constraints. For the 1-stage direct-flow design, the overall capital cost was predicted to decrease by 14%. For the 2-stage design the decrease was predicted to be 12%. The relative decreases in cost were larger when only the stack was considered (17% and 18%, respectively); however, it is clear that the stack cost itself is not the only driver of capital cost in the ED systems considered, as the supporting hydraulic network contributes to a bulk of the cost.

### Cost sensitivity to voltage constraint

As discussed above, the constraint placed on voltage was a design decision made with the goal of meeting manufacturing as well as technical requirements. Given that the $V_{max}$ constraint was active (i.e. limited the design) in both the 1- and 2-stage direct-flow continuous systems, it is useful to explore how relaxing this constraint would affect the objective value to assess whether the constraint is excessively restrictive and may be preventing us from achieving a lower capital-cost solution. In order to assess this, we again used the assumptions described in Section 4.3, however, we adjusted the value of $V_{max}$. Figure 4-7 shows the resulting normalized (percentage) change in cost with a relative change in the maximum voltage. While reducing the maximum voltage is seen to have a strong influence on the cost, increasing the voltage did not. This is likely due to the coupling with limiting current, which was the second active constraint for all the optimal continuous designs.

The recovery ratio was a second inflexible constraint during the design optimization. Upon performing a similar cost sensitivity analysis, it can be seen that there is a relative

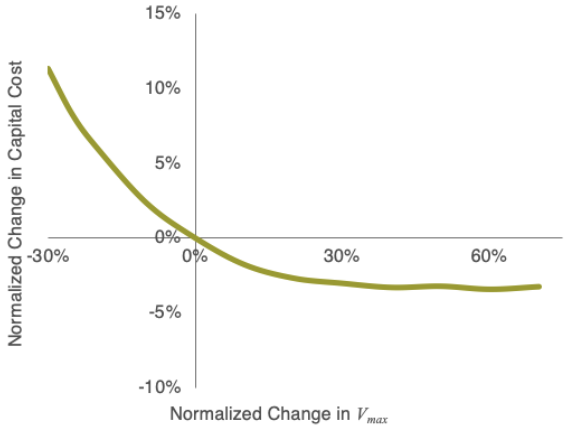


Figure 4-7: Cost sensitivity to the voltage constraint shows that the same increase in cost from a reduction in the limit does not translate to an equal cost savings if the limit is increased by the same percent.

cost increase for the cost optimal designs of lower recovery ratio targets.

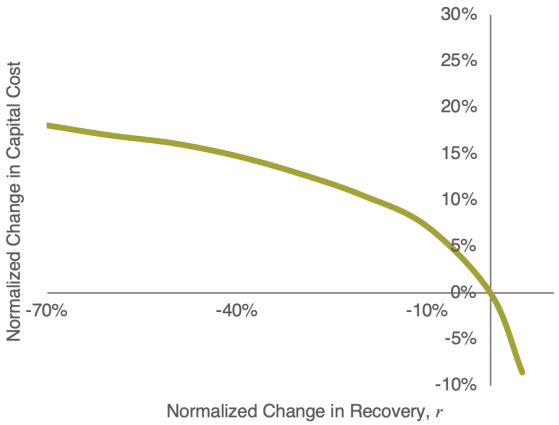


Figure 4-8: Cost sensitivity to the recovery ratio demonstrates that higher recovery ratios are advantageous with respect to cost.

### Cost sensitivity to spacer geometries

The geometry of the spacer is known to be linked to many aspects of ED performance. Spacers are selected during the design phase so understanding the relative importance of the main parameters is important to selecting an ideal spacer. Of particular interest here is how three key parameters of the spacer (thickness $h$, volume porosity $\epsilon$, and area porosity $\phi$) impact the minimum capital cost stack for a 1-stage direct-flow design. It is difficult to find

a spacer material that will result in a minimized cost along all these dimensions, however, comparing the effect of these parameters individually allows a designer to understand the relative impacts of changes in mesh specification.

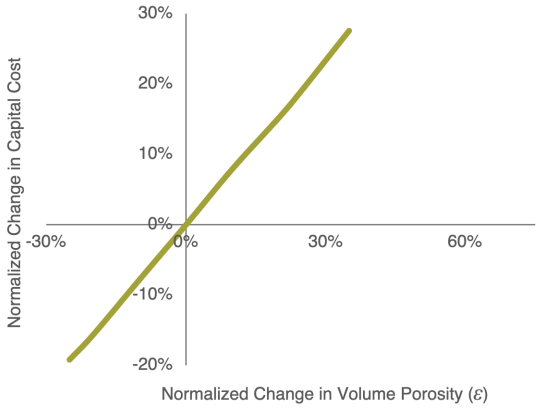


(a) Cost sensitivity to the volume porosity of the spacer demonstrates a roughly linear trend in fractional cost increase with fractional changes in the volume porosity.

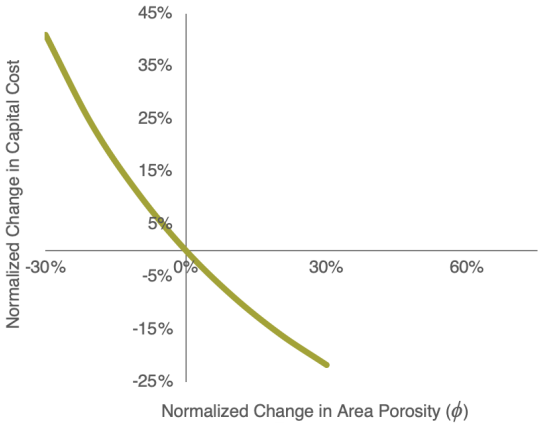


(b) Cost sensitivity to the area porosity of the spacer

Figure 4-9: Cost sensitivity to mesh porosity characteristics

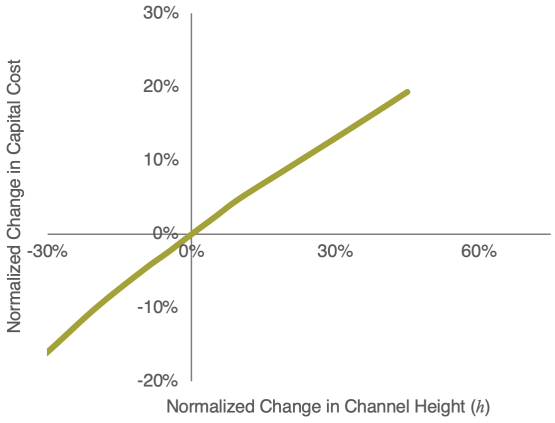


Figure 4-10: Cost sensitivity to the thickness of the spacer

# Chapter 5

# One-stage prototype validation

The design trade off study described above is limited in that its utility is as a comparative tool to assess the differences between architectures. While it overcomes the difficulty of current literature not having a unified point of comparison to assess the different system variants together, it can not be used as a direct predictor of cost or function without more detailed experimentation with the proposed architecture. Therefore, a prototype system was manufactured (Fig. 5-1) and assessed against the design requirements of Table 1.1.

## 5.1 POU ED prototype

The prototype was a reversal-enabled 1-stage direct-flow continuous architecture as proposed in Fig. 2-6. For this prototype, a thinner mesh was chosen than was modeled in Section 4.3 in order to decrease the area required for desalination by increasing the mass transfer (Eq. 2.5) and resulting current limit (Eq. 2.4). Table 5.1 includes the key material parameters of the prototype system. The target flow rate was also adjusted to 13.5 L/h for the prototype. This is lower than the 15 L/h upper bound used in the design comparison but remains within the requirement of Table 1.1 and provides a margin for minor flow rate fluctuations during operation.

We used the same stack models described in Section 4.3.2 to determine a cost-optimal

flow path length (31 cm) and width (2 cm) for the 13.5 L/hr flow rate and design requirements of Table 1.1. Fabrication of this custom geometry was accomplished by the spacer manufacturing process described in Section 3.1.1. In manufacturing the spacers used in the final prototype, the geometry of the spacers was analyzed and outliers from the population were not included in the final build. Spacers were measured in four locations and visually inspected to ensure there were not gaps or imperfections that would cause the flow to be rerouted between channels or to leak from the stack. After all the measurements were taken, the average thickness of spacers used in the tested stack was 194 $\mu m$ with a standard deviation of 15 $\mu m$ and an inter quartile range (IQR) of 33 $\mu m$. Spacers with individual measurements that exceeded 1.5 times the IQR of the full population were not included in the final build. There was a scrap rate of 14.8% during fabrication.

The CEM and AEM were cut to the required size from commercially available IEMs manufactured by SUEZ Water Technologies and Services. Endcaps were machined from polycarbonate (Fig. 5-1) and electrodes were purcased per required specifications from Shaanxi Yunshong Metal Technology Co.

The resulting stack volume (estimated as described in Section 4.3) was 4.5 L and the resulting system cost estimate was $166 USD. The system was design to adapt to changes in feed water salinity using a linear control scheme executed using an Arduino-capable MELIFE ESP-32S development board and an ARCELI boost buck converter (50V, 5A) controlled via a PC. In a fielded POU ED system this control would take place within the purifier with chip-level components.

### 5.1.1 Experimental setup and test protocol

All testing was performed with NaCl solutions of the required salinity to simplify model validations. Time series conductivity data were collected using sensors typical of POU purifiers currently on the market (two-wire analog detectors, 0-1000 mg/L TDS range, ±10% accuracy (Banggood, China)). Due to the narrow accuracy range, these were recalibrated prior

Table 5.1: Configuration of prototype 1-stage direct-flow continuous system

| Metric | Unit | Value | Material (Supplier) |
|---|---|---|---|
| | | *Configuration* | |
| Valves | - | 6 | 24VDC Solenoid (Malida) |
| Pumps | - | 2 | 1 from POU UV purifier system, 1 Mini Water Pump SS524-1502-2500 |
| | | *Spacer Mesh Properties* | |
| Thickness | [$\mu$m] | 194±15 | Woven polyester |
| Void fraction | - | 72% | KL-60 100D |
| Area porosity | - | 61% | (Changzhou JC Fabrictec Co.) |
| | | *Flow Channel Properties* | |
| Cell Pairs | - | 46 | - |
| Dimensions | [m] | 0.02 x 0.31 | |
| Total IEM area | [$m^2$] | 0.46 | - |
| Linear velocity | [$\frac{cm}{s}$] | 3.4 | - |
| Pressure drop | [kPa] | 104 | Eq. 2.11 |
| | | *Ion Exchange Properties* | |
| AEM resistance | [$\Omega cm^2$] | 30 [34] | AR204SZRA (SUEZ) |
| CEM resistance | [$\Omega cm^2$] | 30 [34] | CR67HMR (SUEZ) |
| Electrode area | [$cm^2$] | 69 | Ru-Ir coated Ti (Shaanxi Yunshong Metal Technology Co.) |

to each trial based on the feed salinity. Characterization tests, static testing, and calibration of the two-wire sensors relied on Myron L Ultrameter (accuracy ±1%) to characterize the conductivity of the solution. Flow rates were measured via manual volume collection over a specified time interval and extrapolated to the L/h rate. Hoses and fittings standard to RO POU purification systems were used wherever possible in the test setup. Fig. 5-2 shows the layout of the experimental setup. The semi-rigid hoses used in this configuration ensured the minor losses from the hydraulic network stayed constant throughout the course of all testing performed.

To understand the desalination capability of the as-built prototype, the mass transfer properties of the stack were first characterized to determine the limiting current over a range of flow rate and feed salinity levels with approximately 50% recovery. Fig. 5-3 shows a sample curve fit that was used to determine the point of limiting current during experimental

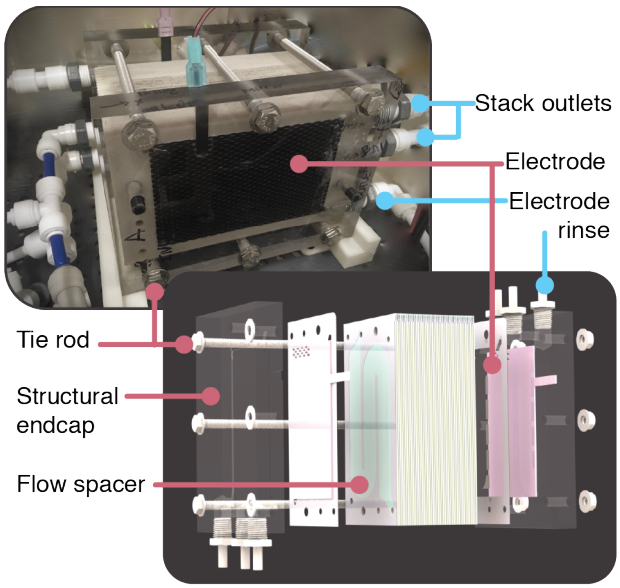


Figure 5-1: Assembled 1-stage direct-flow continuous POU ED prototype unit in test and CAD schematic view expanded to show internal features.

trials. The inflection point was selected visually. For trials where the corner between the two sections was more shallow, data points that did not follow the clear linear trend of the data in either regime were excluded from the fit.

All characterization tests were performed in each of the two EDR 'positions' (inverting the anode and cathode) and tagged to allow for comparisons between results in the two configurations. Before each test, the system was equilibrated at the testing salinity by circulating $\geq$2 liters of water at the salinity of the next test. The pH of the diluate stream was monitored throughout to verify whether water splitting was occurring in the diluate channel boundary layer, indicating the system was exceeding $i_{lim}$.

## 5.2 Desalination experimental results

Table 5.2 shows the results of the POU ED prototype compared to the design requirements and initial predictions from the theoretical model presented herein. The experimental salt reduction was 37$\pm$5% for the measured salinities, 41$\pm$6% that predicted by the design model. Flow characteristics were met in the experiments. The discrepancy between the model and

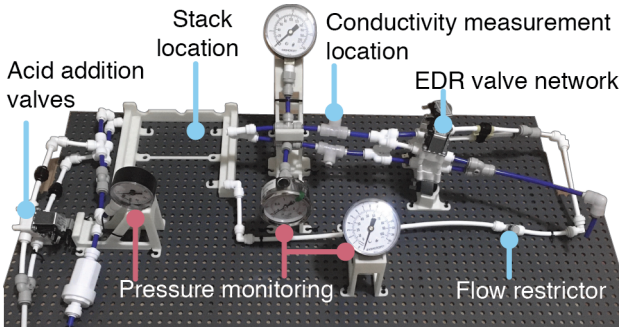


Figure 5-2: POU ED experimental setup depicting the use of semi-rigid, 1/4 inch RO tubing, pressure gauges, and conductivity measurement points. Gauges were placed to minimize minor hydraulic losses when recording the stack pressure loss, and the conductivity readings were made near the stack to reduce lag in the data. Blue components would be included in an installed system.

results indicated some of the input parameters may have been inaccurate; the following subsections explain why and how the model accuracy was improved.

Table 5.2: Experimental results of the prototype 1-stage direct-flow continuous system.

| Metric | Target | Theoretical Prediction | Experimental Results |
|---|---|---|---|
| TDS reduction from 500 mg/L | -90% | 50 mg/L | 340 mg/L (-40±0.3% from feed) |
| TDS reduction from 1500 mg/L | -90% | 150 mg/L | 940 mg/L (-38±6% from feed) |
| TDS reduction from 2500 mg/L | -90% | 738 mg/L | 1610 mg/L (-37±6% from feed) |
| Flow Rate | 10 L/h | 13.5 L/h | 13.5±0.5 L/h |
| Recovery | $\geq$ 90% | 90% | 90±3% |

Fig. 5-4 shows the results of the static tests over multiple operating points compared against the model with correlated input parameters, and contrasted against the original (as designed) model prediction. Above the design target for feed salinity (1500 mg/L) the as-designed model is unable to meet the 90% reduction target because the 24 V constraint is active, leading to the prediction of 738 mg/L product water for a feed of 1500 mg/L. By contrast, mass transport to the IEM is the limiting factor in the characterized as-built system, so the 24 V constraint does not cause an inflection as salinity increases and the results follow an approximately linear trend as feed salinity increases.

This discrepancy between the modeled and measured desalination is a direct result of

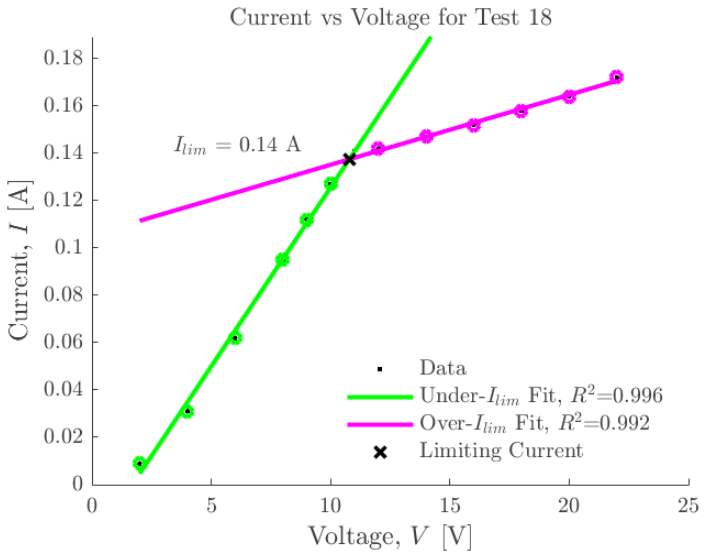


Figure 5-3: The intersection of two linear fits above and below the limiting current point is used to determine the estimated applied current where the stack begins to split water along a portion of the flow path.

decreased current carrying capacity across the flow channels. Two possible explanations for this are 1) incorrect assumption of mass transport, in particularly mixing as described by the Sherwood number and 2) reduced planar area in which ions can flow due to air entrapment in the system.

### 5.2.1 Effective Sherwood number

Recalling that the relation between $Sh$ and the flow parameters, $Re$ and $Sc$, is determined experimentally, we chose to characterize our system in order to determine the mass transfer behavior specific to the as-fabricated prototype. In our characterization we held the exponent on $Re$ and $Sc$ constant, and fit a new leading coefficient to the full equation (Eq. 2.9).

The computational system model was used to determine what coefficient would result in the same integrated current ($I_{app}$) for the stack at the point where the end of the flow path first attained the limiting current density ($i_{lim}$). This point was selected given the clear indication in the experimental data of when $i_{lim}$ is attained. Mathworks MATLAB was used to optimize what leading coefficient would minimize the sum of squared residuals error

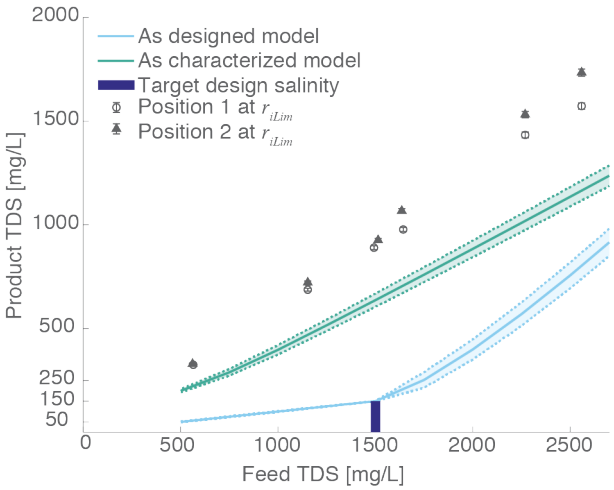


Figure 5-4: Static desalination performance of POU prototype. The measured salinity at $i = i_{lim} r_{iLim}$ differed by 13% on average (maximum 23%) between the two EDR positions. The data presented are for operation of the stack with $r_{iLim} = 0.7$. The salinity target used in designing the system is marked at 1500 mg/L and the inflection in the model curve due to the voltage constraint is apparent above this point. Error in the as-characterized model comes from measurement uncertainty of 13.5±0.56 L/hr for flow rate and 90±3% on the recovery ratio.

between the experimentally measured and computationally modeled $I_{app}$. No significant difference was observed between the two EDR positions, so the full data set fit was used to determine the updated Sherwood number correlation of $Sh = 0.078 Re^{0.5} Sc^{0.33}$ that was used to generate the 'as characterized' curve of Fig. 5-4.

After performing characterizations on the as-built system, we can see that the experimental results fall above the updated modeling predictions for the functionality of the system by >20%. This characterization involved limiting current tests performed at multiple flow rates and with feed salinities ranging around the design target. For each fit, the data were segmented visually into regions above and below limiting current and linear regressions were applied to determine the intersection point of these curves (see Fig. 5-3 of the supplemental information section).

### 5.2.2 Performance impact of air entrapment in the flow spacer

If the observed performance degradation is due to air entrapment, the observed performance can be approximated as a percent reduction in area over which the current is allowed to travel. Using Eq. 2.4, we note that $i_{lim}$ is a current *per unit area*. We therefore approximate the relation between measured limiting current $I_{app,lim}$ and $i_{lim}$ as

$$I_{app,lim} \approx \iint_{LW} i_{lim} \approx i_{lim} LW. \tag{5.1}$$

If we assume that mass transport of ions to the IEM surface is not the limiting factor experience over a majority of the stack, $i_{lim}$ is constant and the discrepancy between the measured and modeled $I_{app,lim}$ can be described as

$$\frac{I_{app,lim,meas}}{LW_{meas}} \approx \frac{I_{app,lim,design}}{LW_{design}}. \tag{5.2}$$

If air enters a *single* cell pair within the stack, we hypothesize this would create a decrease in current flow in the obscured region even in subsequent cell pairs where the air was not present. This could explain a reduction in current while flow properties (and therefore mass transfer) are not as significantly impacted because the 45 remaining cell pairs would see a relatively small impact from an air obstruction of one cell pair. Across the data collected, on average an obstruction of 68±8% of the normally open flow path would cause the observed results.

Assuming that air entrapment is at least a contributing factor in the decreased desalination performance, there are two ways to diminish this issue. First, during the stack design phase, alternate (thicker) spacers with comparable open area could be considered in order to better allow air to exit the system and not become trapped by surface tension in the narrow voids of the spacer. Second, during manufacturing and system integration, controls could be put in place to reduce the likelihood of air entering the system (e.g. by constructing the

stacks while submerged in water or shipping the stacks wet as is done with RO membranes) and to prevent air from reaching the stack during operation (e.g. through the use of bleed valves).

## 5.3 Experimental pressure loss comparison

Three models of pressure drop were assessed for the system we built to validate the design study. All three were selected from Wright et al.'s [21] paper on ED stack modeling for their correspondence to the systems they analyzed. In addition to the model from Ponzio et al, (Eq. 2.11), additional models proposed by Pawlowski et al. [37] and Gurreri et al. [38] for woven spacers were considered. The friction factors for the latter two models are given below and can be directly substituted into Eq. 2.11 in their given form.

$$f_{Ponzio:Re<61} = \frac{1400}{Re} \tag{5.3}$$

$$f_{Pawlowski} = \frac{24(2 + 8(1 - \epsilon))^2}{\epsilon^3 Re} \tag{5.4}$$

$$f_{Gurreri} = 4\frac{50.6}{\epsilon^{7.06} Re} \tag{5.5}$$

Similar to Wright et al. [21], we observed a better correspondence to the Gurreri model for the smallest (fewest cell pair) system that we tested as can be seen in Fig. 5-5. The stack showing this correlation in our data used the same flow path geometry as the eventual full-size prototype, however, it had 15 cell pairs instead of the full 46. When the additional cell pairs were added, the system corresponded much better to the Ponzio or Pawlowski models.

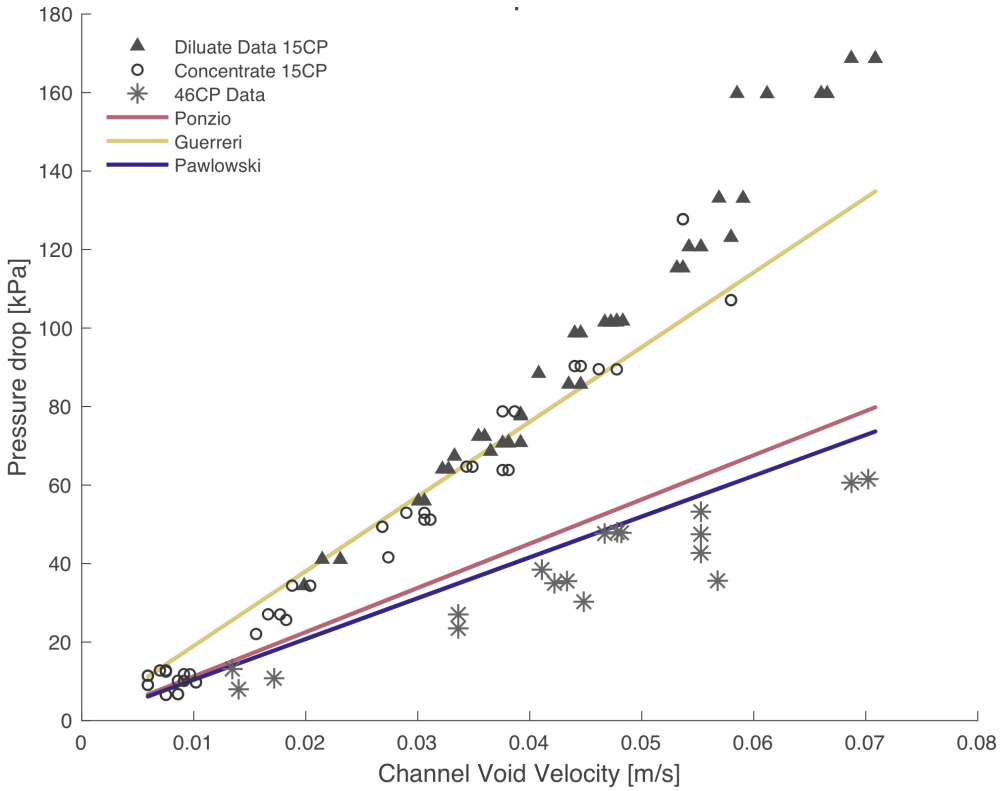


Figure 5-5: Comparison of measured pressure drop verses modeled pressure drop predictions for two iterations of the prototype system.

## 5.4 Operational adaptability

Responding to the requirement that the system be responsive to instantaneous changes in feed water salinity, time series experiments were performed to examine the system response to dynamic feed salinity. After a target TDS was selected (e.g. 10% of the feed), a linear control scheme was used to track the initial voltage/current to within a target band. Fig. 5-6 demonstrates the response of the system to a change in feed salinity (initial portion of the curve) and a polarity reversal (at 35 s). The target output in this trial was maintained at 70% of the feed TDS and recovery was 92%.

The time series plot shows over-shooting behavior both when the salinity increases and when it decreases. Additional refinement of the controller will be necessary to more rapidly meet a TDS change and supply product water that does not significantly disrupt the salinity of stored product water in the system. However, rapid changes in feed salinity would not be

common in practice, as they are more likely to drift over time with environmental changes. This is feasible with the implementation of PID control and improved initial targeting based on approximations from the advanced system models described previously.

The large error range on the analog sensors commonly used in POU RO systems can also bee seen in Fig. 5-6. Some level of customer input may be required in order to tune the preferred level of desalination if the sensors drift over time and cease to produce the expected results. This is typical of RO POU purifiers on the market today. Recalibration to test solutions would also be required during service visits in order to ensure that a shift in the input conductivity reading would not cause the applied current to the stack to exceed the current limit threshold.

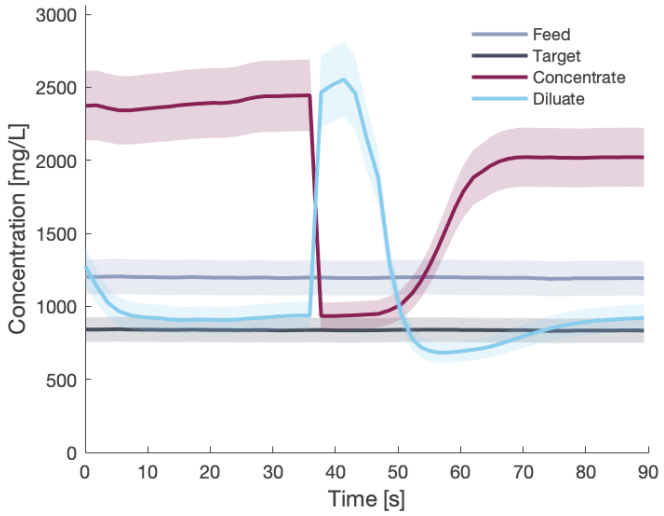


Figure 5-6: Linear control provides confidence that active feedback to the stack allows the system to adjust to changes in feed water concentration while maintaining a fractional salt cut, here set to 70%. This is maintained through a reversal of the EDR system at ~35s.

## 5.5 Packaging volume mock-up

Figures 5-7a and 5-7b demonstrate the fit of the proposed system architecture within an existing commercially available RO purifier housing. This demonstrates a POU ED system could meet the packaging design requirement laid out in Table 1.1. The stack volume was

modeled after the prototype system (not the design-study system of Section 4.3). RO components have been removed and the pump has been replaced with a smaller model that is better suited to the pressure drop across the ED stack. The back of the unit accommodates the acid storage reservoir and acid pump and valves. The front view includes the stack and the additional valves necessary for reversing the outputs of the system. The pump is not visible as depicted here but is installed under the stack in this view. Note that the valve

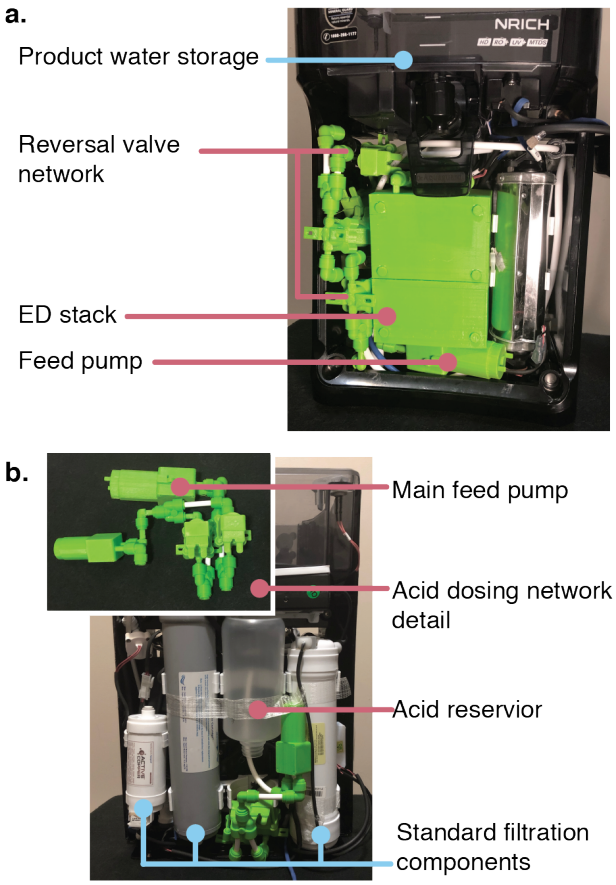


Figure 5-7: Volumetric models of all required components additional to the ED system are included in a commercially available wall-mount purifier on the market from Eureka Forbes. **a**. The stack and hydraulic network of valves necessary for reversal is contained by volume in place of the standard RO pump. The feed pump necessary for the ED system is small enough to fit in a gap underneath existing components. **b**. The acid storage container and the miniature pump necessary to dispense the acid is located in place of the RO cartridge on the back side of the device.

network on the stack output could not be plumbed into the rest of the system in the volume study as shown. Furthermore, the front edge of the stack as proposed would interfere with

the purifier front cover by ≈0.5 cm given the location of the mid-plane attachment plate within the RO purifier. While all the components have sufficient available volume to fit, the interior geometry of the purifier will require modification to allow for the necessary hydraulic connections to be made.

THIS PAGE INTENTIONALLY LEFT BLANK

# Chapter 6

# Discussion and conclusions

## 6.1 Discussion

As presented here, POU ED offers the opportunity to rethink conventional ED system design. The novel, direct-flow continuous design proposed allows for lower cost and complexity systems than have been previously proposed for POU ED. This novel system architecture showed further promise as the most capital-cost optimal POU ED design in the trade off analysis performed in Section 4.3. Indian customers have previously indicated a willingness to pay over USD 200 for high recovery devices [6]. While the overall capital cost of the refined system design is higher than the capital cost of current RO systems, it falls near the previously predicted willingness to pay. At the same time, households using a high-recovery ED purifier would save additional cost in lower water use rates. The estimated capital cost would likely come down as the stack build costs benefits from economies of scale, however it is our belief that the cost of a POU ED system will remain above current RO products.

In Section 2.4 we discussed design insights relating to pressure differential and flow rates within a POU ED stack that we were then able to realize in a functional prototype in Section 5. This system was able to operate on a single pump for water circulation, unlike industrial systems that require two pumps. While the desalination was not sufficient to meet the

design requirements, the architecture of the stack presented no indications that it was the cause of the problems observed. Recovery was maintained at 90±1% for >20 L of water and the discrepancy between the positions was minor (within 4%) through multiple system on-off cycles over 7 days, indicating that the system maintained the recovery ratio while also implementing the necessary self-cleaning measures that will make it successful in the long-term. No intermediate storage reservoirs or pumps were required to recover more than 50% of the feed volume as product water. As predicted in the design insights, no membrane damage was observed at the POU flow rates. Further, the packaging volume of the system proposed was sufficiently small to fit (by volume) within a commercial POU purifier housing.

Despite successfully validating the proposed architecture, the desalination performance and installation requirements of the prototype described in Section 5 could still be improved. The volumetric model study of this architecture made clear the value of minimizing component count and volume for any ED stack intended for inclusion in wall-mount POU purifiers. The initial design requirement of volume under 6 L for additional components may more realistically be reduced to ≤5 L to enhance accessibility of components during assembly or maintenance. Identifying commercially available items that can fill the need for two position valves at a comparably low cost will go a long way towards simplifying the bill of materials for even the simplified architecture. Customization of low-cost components (such as the acid storage tank) may also allow usable internal volume to be maximized. Including an acid reservoir with a shape molded to fit into an otherwise unused or inaccessible area of the internal cavity could help capitalize on the space available.

In order to improve the desalination function of the prototype we suggest a reassessment of the material set being used in fabrication. For the same design requirements used to design the prototype, the cost-optimal design for a stack using the same PCCell mesh used in the characterization study would result in a system with a predicted capital cost of 10% greater than with the material set used to construct the prototype ($182 total cost with a stack cost of 20% greater than the prediction with parameters of 5.1). This mesh, when used in the

commercial bench-top system, has previously been shown to align with the mass transfer predictions of Eq. 2.9. Similarly, with parameters of the PCCell mesh, the volume of the stack increases by 20% from 2 L to 2.4 L. Given this mesh has been previously validated and is used in fielded systems, updating the design to use this mesh would likely eliminate the problems encountered with the thinner mesh used here.

With the ability to reject higher salinity waste water, the question of brine management is inevitable. The environmental cost of adding the volumes of brackish water produced by POU ED should be further considered. However, given the relatively small volume compared to other desalination applications (e.g. in agriculture) and given that POU purifiers frequently channel their waste to a municipal drain, mitigation of the increased brackish water should be manageable at the municipal level. This will become a greater issue as the market growth predicted for POU systems is realized.

Even with the work that remains, the potentially massive environmental benefit of implementing POU ED to conserve water warrants continued effort on this topic. As discussed previously, with only 10% adoption of low-recovery POU purifiers in the two highest socioeconomic groups of India, 234 ML of water would be wasted every day [6]. The same adoption rate of 90% recovery ED POU purifiers would save >225 ML/day and leave millions of liters of water available to meet the needs of additional households around India.

## 6.2 Conclusions

The amount of water wasted by commercial POU purifiers in India, combined with their growing adoption rates, provide a compelling case to innovate in the POU water purification space before water scarcity in the region accelerates further. ED provides promise in the form of a water-efficient technology compared to RO. In this work we present a rigorous analysis of the design requirements for a POU ED purifier in order to propose a technological manifestation that meets market and consumer requirements in a affordable, water-saving

product. The main contributions of this work are:

1. a new direct-flow continuous architecture with variable flow rates,
2. demonstrated cost feasibility of POU ED with higher fidelity than previous work, and
3. validation of the architecture proposed via experimental lab tests and a full-size mock-up.

We provide a comprehensive list of design requirements that not only meets the needs of the end user but responds to the production and commercial market pressures that govern the success of a new consumer product. Early integration of Eureka Forbes as a stakeholder in the design process aided in the generation of this list. Through combining a model-based examination of ED systems architectures with insights about ED function that are unique to the POU scale, we were able to show that a previously unexplored ED system architecture exists that better meets these design requirements.

This direct-flow continuous architecture uses a single pump, fewer valves and no intermediate storage tanks, saving cost and reducing complexity compared to the system architecture common to industrial ED. The insight that the diluate and concentrate channels could tolerate different flow rates at the POU scale enabled this direct-flow architecture to be realized. A prototype of this system was able to validate the water conservation, lower pressure requirement, and affordability of the proposed architecture.

While the desalination performance of the POU ED prototype was approximately half that initially predicted in the model, we hypothesize that a different choice of mesh would enable improved desalination without significantly increasing the cost or packaging volume of the system. Further work is needed to characterize the materials of a commercially-ready system.

Table 6.1: Acronyms and variables

| Abbreviations | Meaning |
|---|---|
| CC | Capital Cost |
| $C$ | Concentration |
| $C^b$ | Concentration in the bulk |
| $C_{d/c}$ | diluate or concentrate |
| $D_{aq}$ | Diffusion coefficient |
| ED | Electrodialysis |
| EDR | Electrodialysis Reversal |
| $F$ | Faraday constant |
| $h$ | Channel height |
| $i_{lim}$ | Limiting current |
| $k$ | Mass transport number |
| $L$ | Flow path length |
| LSI | Langelier Saturation Index |
| $N\#$ | Number of cell pairs in stage(#) |
| OC | Operational Cost |
| $P$ | Pressure |
| POU | Point of use |
| $Q_{prod}$ | Production flow rate |
| $Q$ | Cell pair flow rate |
| $r_{iLim}$ | Limiting current threshold ratio |
| $R_{mem}$ | Membrane resistance |
| RO | Reverse osmosis |
| $Sh$ | Sherwood number |
| SV | Solenoid valve |
| TDS | Total dissolved salts |
| $u_v$ | Void channel velocity |
| $V\#$ | Voltage applied to stage(#) |
| $W$ | Flow path width |
| $z$ | Ion valency |
| $\epsilon$ | Void fraction of spacer |
| $\rho$ | Density of feed water |
| $\phi$ | Area porosity of spacer |
| $\eta_{pump}$ | Efficiency of the pump |

THIS PAGE INTENTIONALLY LEFT BLANK

# Appendix A

# 2-stage intermediate concentration validation

After obtaining the cost optimal design of the 2-stage system, I was able to validate the analytical result of Equation 4.4 for the intermediate concentration of the stack. I was able to demonstrate that for the optimal cell pair distribution between the first and second stages, the geometric mean is the convergence point where the least amount of the flow path length will be over the limiting current (i.e. the most cost effective design to achieve operation within the design requirements occurs under these conditions. Fig. A-1 demonstrates this for the cost-optimal case. Three path lengths were tested for 7, 10, and 13 cell pairs in the second stage, and the intermediate concentration was incremented between the feed and product concentration. Allowing the simulation to apply the required voltage to achieve the target intermediate and feed salinities.

For the higher and lower cell pair counts, the non-optimal cases favor increased amount of desalination in the stage that has a relative membrane 'surplus', shifting the inflection point to a higher intermediate salinity in the case of greater membrane area in stage 2 ($N2$=13), and lower $C_{int}$ when less membrane area is present ($N2$=7).

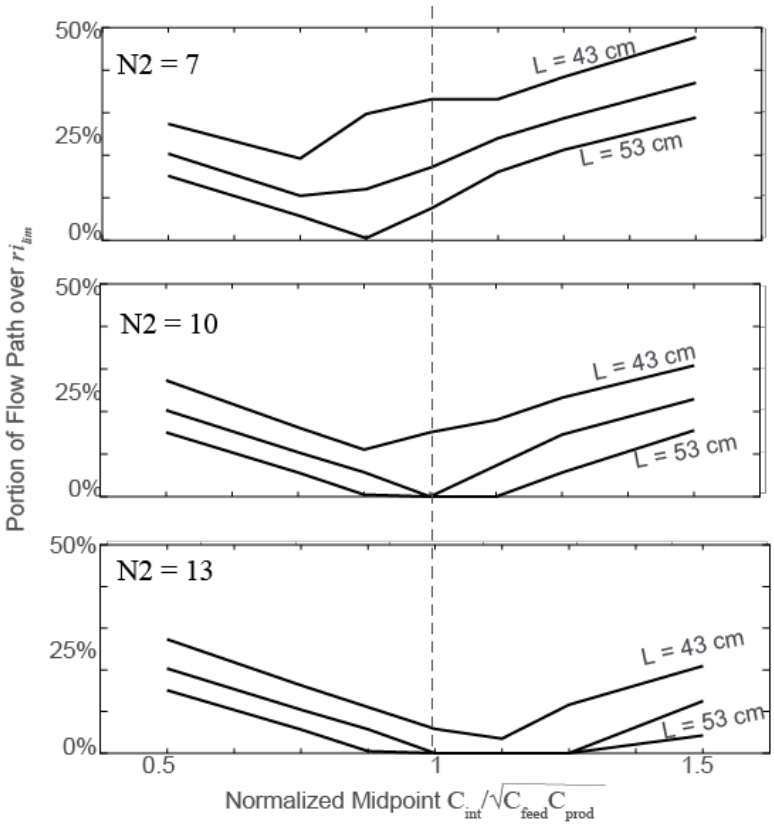


Figure A-1: Manually varying the midpoint salinity show convergence on the geometric mean as the intermediate salinity with the least amount of flow path over the current threshold across a range of path lengths and number of cell pairs in the second stage, $N2$. Convergence is best at the optimal capital cost design (minimum membrane area). Path width 20 mm, 13 cell pairs in the first stage.

# Appendix B

# Capital cost sourcing

A complete list of sources for the capital cost of a POU purifiers is in Table B.1, below.

Table B.1: The capital cost estimates are based on a combination of commercially available figures for component parts and quotes received by the authors while constructing the design.

| Component | Unit cost [$US] | Source |
|---|---|---|
| *Fixed purifier costs* | | |
| Housing | 11 | Material cost estimate for injection molding without amortized tooling costs. Assuming at-volume production |
| Water storage within unit | 5 | AliExpress Runing road Store: 15L Water Plastic Bucket Home Water Storage Reusable Plastic Water Bottle Gallon Jug Storage Container Outdoor BPA-Free Hot Sale |
| Hydraulic piping and network | 4 | AliExpress China Pneumatic & Industrial Market - AliExpress: Store |
| Power supply | 6 | AliExpress Walking Koala Store: 12V 5A 5 amp 60W DC EU POWER Supply ADAPTER Transformer LED Strip Light for 5050 3528 #15 |
| Electronic circuitry | 9 | Based on prototype fabrication costs priced out to bulk order quantities. $1 PCB, chip-level component costs |
| Conductivity meter | 1 | Half the cost of a packaged handheld TDS meter on the market: AliExpress Honestycentre Store: Portable Pen Portable Digital Water Meter Filter Measuring Water Quality Purity Tester TDS Meter |
| Sediment filter | 2 | AliExpress Smart Home Life Store: Water Purifier 10 Inch 4pcs 1 Micron Sediment Water Filter Cartridge PP Cotton Filter Water Filter System |
| Carbon filter (2X) | 2 | AliExpress Make It Happen Store: Activated Carbon Home Kitchen Faucet Tap Water Clean Purifier Filter Cartridge High Quality and AliExpress Smart Home Life Store: Water Systems Replacement Pre-Filter SET 3 Stage Whole House Water Filter PP Sediment Carbon Filter Cartridge Reverse Osmosis |
| UV sanitizing lamp | 4 | AliExpress GuanXia Store: Ultraviolet Ozone Lamp Quartz Glass Screw Light Bulb Disinfection Light For Bathroom Bedroom Living Room UV-Licht Sterilisator |
| *Total fixed cost:* | *47* | |
| *Costs of an ED system* | | |
| Water pump | 16 | AliExpress Coronwater Official Store: Coronwater 75gpd Water Filter RO Water Booster Pump 2766NH Increase Reverse Osmosis System Pressure Cost estimation based on the price of RO pumps for the purposes of estimation, a lower-cost, lower-pressure pump can be exchanged into the ED system for cost savings given the lower pressure of ED operation. |
| Solenoid valves | 2.5 | AliExpress Shop2960077 Store: Water Inlet Valve AC220V 12V 24VDC NO NC Plastic Solenoid Valve 1/4" 3/8"OD TubeHose Connection forRO Reverse Osmosis PureSystem |
| Miniature pump for acid dosing | 5 | AliExpress Shop5366192 Store 12V DC Small 370 Water Pump With DC Motor Low Noise Large Water Flow 0.4-1.2L/min For Drinking Mini KLC Diaphragm Vacuum Pump |
| Stack-specific electronics | 4 | Estimated by the authors from quotes used in manufacturing the prototype set-up |
| Conductivity meter | 1 | (one additional sensor to that listed in purifier costs section, see above) |
| ED stack hardware | 4 | Estimated by the authors from quotes used in manufacturing the prototype with assumption of savings for at-volume production |
| *Variable costs of the ED stack* | | |
| Electrodes | 2000/$m^2$ | Quote obtained by the authors [35] |
| Membranes | 40/$m^2$ | Quote obtained by the authors [36] |
| Spacers | 0.06/$m^2$ | Estimate based on capital cost of mesh. Exact cost will depend on production volume. |

# Appendix C

# Complete results of comparison

The table below details the metrics of comparison across the full design space considered during the trade off (feed water salinities of 500 and 2500 mg/L). Many of the same trends between the three designs observed at 1500 mg/L are apparent at 500 and 2500 mg/L.

The cost of the two direct-flow continuous architectures is seen to increase as the salinity increases. This increase is driven directly by the requirement to accommodate higher feed salinities: the membrane and electrode area required to accommodate the potential for more saline feed is higher, adding to system costs. By contrast, the cost of the batch system stack is constant across all input salinities. This is a result of the fixed *percent* reduction in salt content for all the feeds and therefore the same ratio of $C_p/C_f$. The added costs of a larger batch system is derived purely from the added cost of the acid required to meet the LSI threshold for the increased salinity concentrate.

Table C.1: Architecture comparison results highlighting key differences between the systems for all feed salinities assessed.

| | | 500 mg/L feed | | | 1500 mg/L feed | | | 2500 mg/L feed | | |
|---|---|---|---|---|---|---|---|---|---|---|
| | | Batch | Direct Continuous | | Batch | Direct Continuous | | Batch | Direct Continuous | |
| | | | 1-Stage | 2-Stage | | 1-Stage | 2-Stage | | 1-Stage | 2-Stage |
| Capital Cost | [US$] | 202 | 166 | 186 | 202 | 195 | 209 | 203 | 218 | 234 |
| Volume | [L] | 8.5 | 4.5 | 5.5 | 8.5 | 5.1 | 5.8 | 8.5 | 5.6 | 6.2 |
| Acid volume | [L/6 months] | 0.1 | 0.1 | 0.1 | 1.1 | 1.1 | 1.1 | 2.5 | 2.5 | 2.5 |
| Cell Pairs | - | 30 | 42 | 34 | 30 | 39 | 23 | 30 | 36 | 18 |
| Electrode Area | [$cm^2$] | 86 | 74 | 69 | 86 | 115 | 109 | 86 | 151 | 149 |
| SEC | [$\frac{kWh}{m^3}$] | 0.4 | 0.1 | 0.2 | 1.1 | 0.35 | 0.7 | 1.7 | 0.6 | 1.5 |

# Bibliography


[1] Central Ground Water Board Government of India. *National Compilation on Dynamic Ground Water Resources of India*. Number July. 2017.

[2] World Health Organization. Guidelines for Drinking-water Quality FOURTH EDITION WHO Library Cataloguing-in-Publication Data Guidelines for drinking-water quality-4 th ed. Technical report, World Health Organization, Geneva, 2011.

[3] Frost and Sullivan. Indian Water Purifiers Market, FY2018. PA12-25. Technical report, Frost and Sullivan, 2018.

[4] Steve Graves. Household Water Filter Evaluation Supply Chain Scalability Report. pages 1–22, 2015.

[5] Sahil R Shah and Amos G Winter. Evaluating the Production and Exergetic Performance of Point-of-Use Reverse Osmosis Devices for Brackish Water Desalination. 2020.

[6] Catherine L O Connor. *Decentralized Water Treatment in Urban India, and the Potential Impacts of Reverse Osmosis Water Purifiers*. PhD thesis, Massachusetts Institute of Technology, 2016.

[7] Shagun Kapil. Down to Earth - centre's new draft for RO systems not what NGT asked for.pdf, 2020.

[8] Natasha C. Wright and Amos G. Winter. Justification for community-scale photovoltaic-powered electrodialysis desalination systems for inland rural villages in India. *Desalination*, 352:82–91, 2014.

[9] Laurent Bazinet. Electrodialytic phenomena and their applications in the dairy industry: A review. *Critical Reviews in Food Science and Nutrition*, 45(4):307–326, 2005.

[10] Luigi Gurreri, Alessandro Tamburini, Andrea Cipollina, and Giorgio Micale. Electrodialysis Applications in Wastewater Treatment for Environmental Protection and Resources Recovery: A Systematic Review on Progress and Perspectives. *Membranes*, 10(7):146, 2020.

[11] T. Scarazzato, Z. Panossian, J. A.S. Tenório, V. Pérez-Herranz, and D. C.R. Espinosa. A review of cleaner production in electroplating industries using electrodialysis. *Journal of Cleaner Production*, 168:1590–1602, 2017.

[12] H. Strathmann. Electrodialysis, a mature technology with a multitude of new applications. *Desalination*, 264(3):268–288, dec 2010.

[13] Kishor G. Nayar, Prithiviraj Sundararaman, Catherine L. O'Connor, Jeffrey D. Schacherl, Michael L. Heath, Mario Orozco Gabriel, Sahil R. Shah, Natasha C. Wright, and Amos G. Winter, V. Feasibility study of an electrodialysis system for in-home water desalination in urban India. *Development Engineering*, 2(December 2016):38–46, 2016.

[14] Sahil R. Shah, Natasha C. Wright, Patrick A. Nepsky, and Amos G. Winter. Cost-optimal design of a batch electrodialysis system for domestic desalination of brackish groundwater. *Desalination*, 443(April):198–211, 2018.

[15] Sreekumaran Thampy, Girish R. Desale, Vinod K. Shahi, Babubhai S. Makwana, and Pushpito K. Ghosh. Development of hybrid electrodialysis-reverse osmosis domestic desalination unit for high recovery of product water. *Desalination*, 282:104–108, 2011.

[16] Eureka Forbes Ltd. Conversations between the authors and Eureka Forbes Ltd., January 2019. Bangalore, India.

[17] Consumer Voice. Packaged Drinking Water / Mineral Water. *Consumer Voice*, pages 10–20, 2016.

[18] Frank Van Weert and Jac Van Der Gun. SALINE AND BRACKISH GROUNDWATER AT SHALLOW AND INTERMEDIATE DEPTHS: GENESIS AND WORLD-WIDE OCCURRENCE. In *IAH Congress*, Niagra Falls, 2012.

[19] Phillip Murray. *Electrodialysis and Electrodialysis Reversal - Manual of Water Supply Practices, M38 (1st Edition)*. American Water Works Association (AWWA), Denver, CO, 1995.

[20] Sahil R. Shah. Cost-optimal design of a household batch electrodialysis desalination device. Master's thesis, Massachusetts Institute of Technology, 2017.

[21] Natasha C. Wright, Sahil R. Shah, Susan E. Amrose, and Amos G. Winter. A robust model of brackish water electrodialysis desalination with experimental comparison at different size scales. *Desalination*, 443(April):27–43, 2018.

[22] J. M. Ortiz, J. A. Sotoca, E. Expósito, F. Gallud, V. García-García, V. Montiel, and A. Aldaz. Brackish water desalination by electrodialysis: Batch recirculation operation modeling. *Journal of Membrane Science*, 252(1-2):65–75, 2005.

[23] C. P. Koutsou, S. G. Yiantsios, and A. J. Karabelas. A numerical and experimental study of mass transfer in spacer-filled channels: Effects of spacer geometrical characteristics and Schmidt number. *Journal of Membrane Science*, 326(1):234–251, 2009.

[24] M. Shakaib, S. M.F. Hasani, and M. Mahmood. CFD modeling for flow and mass transfer in spacer-obstructed membrane feed channels. *Journal of Membrane Science*, 2009.

[25] Vítor Geraldes and Maria Diná Afonso. Limiting current density in the electrodialysis of multi-ionic solutions. *Journal of Membrane Science*, 360(1-2):499–508, 2010.

[26] Francesco Nicolò Ponzio, Alessandro Tamburini, Andrea Cipollina, Giorgio Micale, and Michele Ciofalo. Experimental and computational investigation of heat transfer in channels filled by woven spacers. *International Journal of Heat and Mass Transfer*, 104:163–177, jan 2017.

[27] Floyd H Meller. *Electrodialysis (ED) & electrodialysis reversal (EDR) technology*. Ionics, Incorporated, 1984.

[28] Fernando Valero, Angel Barceló, and Ramón Arbós. Electrodialysis technology-theory and applications. In *Desalination, trends and technologies*. IntechOpen, 2011.

[29] Alice Antony, Jor How Low, Stephen Gray, Amy E Childress, Pierre Le-Clech, and Greg Leslie. Scale formation and control in high pressure membrane water treatment systems: A review. *Journal of Membrane Science*, 383:1–16, 2011.

[30] Sahil R. Shah, Sandra L. Walter, and Amos G. Winter. Using feed-forward voltage-control to increase the ion removal rate during batch electrodialysis desalination of brackish water. *Desalination*, 457:62–74, 2019.

[31] Hong Joo Lee, F. Sarfert, H. Strathmann, and Seung Hyeon Moon. Designing of an electrodialysis desalination plant. *Desalination*, 142(3):267–286, 2002.

[32] Hannah M. Varner, Sahil R. Shah, and Amos G. Winter. The determination of a cost optimal design for a multiple stage continuous electrodialysis desalination device for use in domestic point of use water purification. In *International Design Engineering Technical Conferences & Computers and Information in Engineering Conference*, pages 1–8, St. Louis, 2020. ASME.

[33] Tom Pankratz. Desal was initially driven by DC current and private equity. *GWI*, (January):45–53, jan 2018.

[34] Neil Edwin Moe, John Barber, and Neil Edwin Moe. Making Sense of Electrodialysis Reversal ( Edr ) Plant. In *The International Desalination Association 2019 World Congress*, Dubai, 2019.

[35] Baoji Changli Special Metal Co. Ltd, Platinized Titanium Anode, 2014.

[36] Hangzhou Iontech Environmental Co. Ltd, IONSEP Membranes., 2014.

[37] Sylwin Pawlowski, João G. Crespo, and Svetlozar Velizarov. Pressure drop in reverse electrodialysis: Experimental and modeling studies for stacks with variable number of cell pairs. *Journal of Membrane Science*, 462:96–111, 2014.

[38] L. Gurreri, A. Tamburini, A. Cipollina, G. Micale, and M. Ciofalo. Flow and mass transfer in spacer-filled channels for reverse electrodialysis: a CFD parametrical study. *Journal of Membrane Science*, 497:300–317, 2016.